Molecular mechanisms for metaplasticity in dendritic spines of hippocampal neurons

Ueda, Hiromi

The Graduate University for Advanced Studies, SOKENDAI

School of Life Science

Department of Physiological Sciences

Index

Abstract

Long-term potentiation (LTP) is a long-lasting enhancement in synaptic currents in combination with an enlargement of dendritic spines (structural LTP: sLTP) in the excitatory synapses. The threshold for LTP induction changes in response to neuronal activity, which is termed metaplasticity and contributes to the maintenance of neuronal excitability in hyper-activated neuronal circuits. However, molecular mechanisms for metaplasticity are poorly understood. Here, we investigated metaplastic regulations of sLTP inductions in CA1 pyramidal neurons of cultured hippocampal slices after chronic neuronal excitation using $GABA_A$ receptor antagonists. Glutamate uncaging-induced sLTP was suppressed in the chronically-excited neurons. A reduction in GluN2B-containing NMDAR-mediated Ca^{2+} plays a role in sLTP suppression. Furthermore, using photoactivatable CaMKII, we found that the CaMKII downstream signaling for sLTP was inhibited by chronic excitation. While the reduction in Ca^{2+} influx was independent of protein synthesis, the inhibition of the CaMKII downstream requires it. These findings demonstrate that the two inhibitory mechanisms (i.e., the inhibitions of Ca^{2+} influx and CaMKII downstream signaling) in the signaling for sLTP increase the sLTP threshold in chronically-excited neurons, providing homeostasis of neuronal excitability.

Introduction

Synaptic plasticity is thought to be a cellular basis of memory formation. When animals acquire new information, synapses in their brains change the signal transmission efficiency between neurons. Since this synaptic change in excitatory synapses of the hippocampus is long-lasting (i.e., synaptic plasticity), it might be related to learning and memory. A well-studied form of synaptic plasticity is long-term potentiation (LTP), a phenomenon in which there is a sustained increase in α-amino-3-hydroxy-5-methyl-4-isoxazole propionic acid (AMPA)-type glutamate receptors (AMPARs)-dependent synaptic efficiency. LTP is caused by increased AMPAR on the postsynaptic membrane and glutamate-dependent ion conductance (Derkach et al., 2007; Malinow and Malenka, 2002). These events increase the presynaptic glutamate-dependent postsynaptic firing frequency for promoting neuronal information transmission.

To date, signaling mechanisms for LTP induction in excitatory synapses in rodent hippocampal neurons have been well-studied (Kruijssen and Wierenga, 2019; Nakahata and Yasuda, 2018; Nishiyama and Yasuda, 2015). Presynaptic glutamates bind to N-methyl-D-aspartate (NMDA)-type glutamate receptors (NMDARs) on the dendritic spine membrane. Then, if the NMDARs are relieved from Mg^{2+} blocks under some conditions such as postsynaptic depolarization (Tanaka et al., 2008), Ca^{2+} entries into spines through the NMDARs (Noguchi et al., 2005; Sabatini et al., 2002). Subsequently, the Ca^{2+} binds to intracellular proteins such as Calmodulin (CaM) and triggers numerous Ca^{2+}-dependent signaling (Wayman et al., 2008). Among these, Ca^{2+}/CaM-dependent kinase II (CaMKII) signaling is important because CaMKII activation is necessary and sufficient to induce LTP (Bayer and Schulman, 2019; Giese and Mizuno, 2013; Herring and Nicoll, 2016; Jourdain et al., 2003; Lisman et al., 2012; Lledo et al., 1995; Pettit et al., 1994; Shibata et al., 2021; Yasuda et al.,

2022). When Ca^{2+}/CaM binds to CaMKII, the kinase domain of CaMKII is released from the auto-inhibitory domain. The kinase domain phosphorylates various synaptic proteins associated with AMPARs recruitment to the postsynaptic membrane (Herring and Nicoll, 2016). In addition, it also induces activations of actin regulatory proteins, such as small GTPases that facilitate actin polymerization, leading to an enlargement of the spine (Harvey et al., 2008; Hedrick et al., 2016; Murakoshi et al., 2011). Since this morphological change is long-lasting and provides scaffolds for additional AMPAR insertions into the postsynaptic sites (Matsuzaki et al., 2004; Sinnen et al., 2017; Steiner et al., 2008), it is termed structural LTP (sLTP). Thus, sLTP is a necessary process for LTP expression at dendritic spines. Indeed, previous studies show that spine volumes are well-correlated with postsynaptic AMPAR currents (Govindarajan et al., 2011; Harvey and Svoboda, 2007; Matsuzaki et al., 2001; Matsuzaki et al., 2004).

The stimulus intensity required for LTP induction is shifted in response to the neuronal activity. This phenomenon is called metaplasticity, the Bienenstock, Cooper, and Munro (BCM) theory, or the sliding threshold model (Abraham, 2008; Cooper and Bear, 2012; Keck et al., 2017). Metaplasticity contributes to neuronal homeostasis by adjusting the threshold for LTP induction. Numerous theoretical models predict that LTP enhances neuronal excitability, which thereby increases the probability of additional LTP (Abbott and Nelson, 2000; Litwin-Kumar and Doiron, 2014; Marder and Prinz, 2002; Miller, 1996; Tetzlaff et al., 2011; Turrigiano, 2008; Zenke et al., 2015; Zenke et al., 2013). This positive feedback process results in the network instability of neural circuits. Metaplasticity raises the LTP threshold in response to neuronal excitation, preventing the runaway induction of LTP (Abegg et al., 2004; Moulin et al., 2019). It maintains neuronal excitability within proper levels. Conversely, neuronal inactivation lowers the LTP threshold to compensate for the decreased neuronal excitability (Arendt et al., 2013; Hobbiss et al., 2018; Hochreiter et al., 2015). Metaplasticity is

empirically induced by prolonged neuronal excitation or inhibition. For example, LTP induction by high-frequency electrical stimulation of Schaffer collaterals is inhibited after chronic neuronal excitation by applying a γ-aminobutyric acid type A ($GABA_A$) receptor antagonist into cultured hippocampal slices (Abegg et al., 2004). The electrical induction of LTP is also suppressed in acute slices after chronic optogenetic excitation administered to the ventral hippocampus of freely moving mice (Moulin et al., 2019). From a physiological point of view, pharmacologically-induced epileptic seizures impair LTP accompanying spatial memory deficits (Suarez et al., 2012). As opposed to these, LTP is facilitated in neurons inactivated by prolonged treatments with tetrodotoxin (Arendt et al., 2013; Hobbiss et al., 2018). These observations demonstrate the neuronal activity-dependent metaplastic regulations of LTP.

Metaplasticity is a fundamental system that provides neuronal homeostasis. However, molecular mechanisms for metaplasticity have been poorly understood. One established mechanism is the change of postsynaptic NMDAR subunit compositions (Perez-Otano and Ehlers, 2005; Shipton and Paulsen, 2014; Yashiro and Philpot, 2008). NMDARs are tetramers typically composed of two obligatory GluN1 subunits and two regulatory GluN2 subunits (Cull-Candy and Leszkiewicz, 2004; Liu et al., 2004; Morishita et al., 2007). GluN2A and GluN2B subunits predominate NMDAR subtypes in the forebrain and determine the NMDAR channel property and signaling (Monyer et al., 1994; Sheng et al., 1994; Yashiro and Philpot, 2008). GluN2B-containing NMDARs pass more Ca^{2+} per current unit than GluN2A-containing NMDARs (Sobczyk et al., 2005). Furthermore, GluN2B-containing NMDARs have slower decay kinetics (Erreger et al., 2005; Prybylowski et al., 2002; Sobczyk et al., 2005) and strongly bind to activated CaMKII, leading to persistent CaMKII activations (Bayer et al., 2001; Bayer et al., 2006). These properties imply that GluN2B subunits increase the probability of LTP induction. Indeed, chronic inactivation of single-synapses increases the

number of the postsynaptic GluN2B and lower the threshold for LTP induction by two-photon glutamate uncaging (Lee et al., 2010). While the NMDAR subunit-based metaplasticity has been investigated (Barria and Malinow, 2005; Berberich et al., 2005; Bridi et al., 2018; Morishita et al., 2007; Philpot et al., 2007; Philpot et al., 2001; Quinlan et al., 1999; Tang et al., 1999), contributions of the NMDAR downstream such as CaMKII signaling remain unknown. In addition, structural insights into the mechanisms of metaplasticity have been few. For example, it remains elusive whether chronic neuronal excitation decreases the probability of sLTP induction or not.

To approach the metaplasticity mechanisms, we applied sLTP stimulation at single-spines of chronically excited neurons in cultured hippocampal slices and observed the morphological change of the spines under a 2-photon microscope. We found that glutamate uncaging-induced sLTP was suppressed after prolonged excitation of hippocampal neurons by a $GABA_A$ receptor antagonist bicuculline application for 24 hours. This sLTP suppression was partially dependent on newly-synthesized proteins during neuronal excitation. To address mechanisms of the sLTP suppression, we measured glutamate uncaging-induced Ca^{2+} influx into singlespines. The Ca^{2+} influx was decreased after the bicuculline treatment in a GluN2B-containing NMDAR-dependent but protein synthesis-independent manner. Furthermore, we investigated the contributions of CaMKII signaling to the sLTP suppression using a genetically-encoded photoactivatable (pa)CaMKII (Shibata et al., 2021). paCaMKII activation by two-photon excitation also failed to induce sLTP after the bicuculline treatment, indicating that CaMKII downstream signaling was inhibited in chronically-excited neurons. The suppression of paCaMKII-induced sLTP required protein synthesis, suggesting that the inhibition of CaMKII downstream was an independent mechanism from the Ca^{2+} influx reduction. These results demonstrate the two independent molecular mechanisms (i.e., the inhibitions of Ca^{2+} influx and CaMKII downstream activity)

contribute to the metaplastic regulation of sLTP in chronically-excited neurons. This dual inhibitory mechanism in the signaling for sLTP can prevent runaway sLTP expressions and stabilize neuronal excitability even in hyper-activated neuronal circuits.

Material and Methods

Animals

All the animal procedures were approved by the National Institute of Natural Sciences Animal Care and Use Committee and were performed in accordance with the relevant guidelines and regulations. All the slice cultures were prepared using C57BL/6N mice (SLC, Shizuoka, Japan). This study used dissociated and slice cultures from both male and female pups.

Regents

Bicuculline was purchased from Wako Pure Chemical Industries (Osaka, Japan). SR95531 (gabazine), 4-methoxy-7-nitroindolinyl-caged-L-glutamate (MNI-caged glutamate), and ryanodine were purchased from Tocris Bioscience (Bristol, UK). Anisomycin and NiCl2 were purchased from Sigma-Aldrich (St. Louis, MO, USA). Ifenprodil, NBQX, MCPG, and cyclopiazonic acid (CPA) were purchased from Cayman Chemical (Ann Arbor, MI, USA). AP5 was purchased from Abcam (Cambridge, UK). Nifedipine was purchased from Focus Biomolecules (Plymouth Meeting, PA, USA). ω-conotoxin GVIA and ω-agatoxin IVA were purchased from Smartox Biotechnology (Saint-Egrève, France).

Plasmids

Plasmids containing *CaMKIIα*, *ESARE/d2Venus*, and CaMKII promoter with 0.4 kbp (*CaMKII0.4*) genes were gifts from Y. Hayashi, H. Bito, and M. Ehlers, respectively. Plasmids containing *WPRE3*, *Cre*, *GCaMP6f*, and *hSyn-DIO-EGFP* genes were gifts from Bong-Kiun Kaang, Connie Cepko, D. Kim, and Bryan Roth (Addgene plasmid #61463, #13775, #40755, #50457), respectively. The synthesized gene encoding *the d2Achilles* gene

was purchased from FASMAC (Atsugi, Japan). pAAV-RC-DJ (AAV2/DJ) and pAAV-MCS/pAAV-Helper were purchased from Cell Biolabs (San Diego, CA, USA) and Agilent Technologies (Santa Clara, CA, USA), respectively.

The plasmids, namely pAAV-ESARE-d2Achilles-SV40polyA, pAAV-hSyn-Cre-WPRE, pAAV-CaMKII0.4-tdTomato-P2A-paCaMKII-WPRE3, and pAAV-CaMKII0.4-DIO-Achilles-WPRE3 were constructed by inserting the respective components into the pAAV-MCS. pAAV-CaMKII0.4-FHS-paCaMKII was described previously (Shibata et al., 2021). The CMV-GCaMP6f-P2A-mScarlet plasmid was constructed by inserting GCaMP6f (Chen et al., 2013) and mScarlet (Bindels et al., 2017), together with the P2A (Donnelly et al., 2001) sequence ATNFSLLKQAGDVEENPGP into the modified pEGFP-C1 vector by replacing EGFP (Clontech).

AAV production and purification

A protocol of adeno-associated virus (AAV) vector preparation has been described previously in detail(Lock et al., 2010; Shibata et al., 2021). Briefly, HEK293 cells in dishes were transfected with the plasmids in the ratio 1:1.6:1 (45 µg of a transgene in pAAV, 72 µg of pAAV-Helper, and 45 µg of pAAV-RC-DJ [AAV2/DJ]) using a polyethylenimine method (Lock et al., 2010). Subsequently, the dishes were incubated at 37 °C and 5% CO2 for 96 hours. The collected culture medium was centrifuged and filtered to remove the cell debris. The clarified supernatant containing the AAV was concentrated using a cross-flow cassette (Vivaflow 50, 100,000MWCO, Sartorius; Goettingen, Germany) or Amicon Ultra-15 (100,000MWCO, Merck, Kenilworth, NJ, USA). Iodixanol step gradients were performed as described by Addgene (homepage section: AAV purification by iodixanol gradient ultracentrifugation). The buffer solution of the purified virus was exchanged with phosphate-buffered saline at different concentrations. The titer of AAV was determined by

quantitative polymerase chain reaction using the THUNDERBIRD qPCR Mix (Toyobo, Osaka, Japan). The resultant virus titers typically ranged between 2 × 109 and 2 × 1010 genome copies/μL in the total volume of ~400 μL.

Preparation of organotypic hippocampal slices and gene transfection by AAV and gene gun

Hippocampal slices were prepared from postnatal day 6–9 C57BL/6N mice as described previously (Stoppini et al., 1991). Briefly, the animals were deeply anesthetized with isoflurane, after which the animals were quickly decapitated, and the brains were removed. The hippocampi were isolated and cut into 350 μm sections in an ice-cold dissection medium (250 mM N-2-hydroxyethylpiperazine-N'-2-ethanesulfonic acid, 2 mM $NaHCO_3$, 4 mM KCl, 5 mM $MgCI_2$, 1 mM $CaCl_2$, 10 mM D-glucose, and 248 mM sucrose). The slices were cultured on the membrane inserts (PICM0RG50; Millipore, Darmstadt, Germany), placed on the culture medium (50% minimal essential medium [MEM], 21% Hank's balanced salt solution, 15 mM $NaHCO_3$, 6.25 mM N-2-hydroxyethylpiperazine-N'-2-ethanesulfonic acid, 10 mM D-glucose, 1 mM L-glutamine, 0.88 mM ascorbic acid, 1 mg/mL insulin, and 25% horse serum), and incubated at 35°C in 5% CO_2.

For imaging the dendritic spine morphology, the cultured neurons were transfected by an injection of AAVs using glass pipettes (Narishige, Tokyo, Japan) after 2–6 days in the slice cultures. For Ca^{2+} imaging, cultured neurons were transfected by a gene gun (Scientz Biotechnology, Ningbo, China) using 1.6 μm gold particles coated with plasmids after 8–9 days in slice cultures. For bullet preparation, gold particles (6 mg) and DNA (12 μg) were used in 30 cm long tubes.

Induction of pharmacological neuronal excitation

$GABA_A$ receptor antagonists (10 μM bicuculline and 1–3 μM gabazine) were added to the culture medium after 11–13 days in vitro (DIV). The time of application was then set to 0 for the experiments. The cultured hippocampal slices were incubated in this culture medium for 24 hours at 35 °C in 5% CO_2. Subsequently, the slices were placed in an imaging buffer solution, and the experiment was carried out for up to 3 hours.

Imaging and analysis of spine morphology

Imaging of dendritic spines in hippocampal slice cultures was performed using a custom two-photon microscope. A Ti: sapphire laser (Spectra-Physics, Santa Clara, CA, USA) tuned to 920 nm was used to excite Achilles or d2Achilles proteins. The fluorescence signals of these proteins were collected with a ×60, NA1.0 objective lens (Olympus, Tokyo, Japan) and detected by a photomultiplier tube (H7422-40p; Hamamatsu, Hamamatsu, Japan) through an emission filter (FF01-510/84; Chroma). Signal acquisition and image construction (128×128 pixels) were carried out using a data acquisition board (PCI-6110; National Instruments, Austin, TX, USA) and ScanImage software (Pologruto et al., 2003).

For spine density measurement, three secondary dendrites (50 μm in length from the primary dendrite) were selected and analyzed for each neuron. The spine density was calculated by dividing the spine number by the length of the dendrite. The images were analyzed using ImageJ software (National Institute of Health, Bethesda, MD, USA).

Two-photon glutamate uncaging

To induce sLTP at single-spines, bath-applied 1 mM MNI-caged glutamates were uncaged by a second Ti: sapphire laser at the wavelength of 720 nm (30 trains, 0.5 Hz, 6 ms duration/pulse, 6 mW, measured under an objective lens) near the spine of interest. Since

the focal plane of the imaging (920 nm) and activation (720 nm) lasers were different (~0.7 μm) due to chromatic aberration in the microscope, they were compensated by moving the sample stage along the z-axis (0.3 μm) with piezo stages (PKVL64F-100U; NCS6101C; Kohzu, Kawasaki, Japan) during the glutamate uncaging. The glutamate uncaging was carried out in the imaging buffer solution (136 mM NaCl, 5 mM KCl, 0.8 mM KH_2PO_4, 20 mM $NaHCO_3$, 1.3 mM L-glutamine, 0.2 mM ascorbic acid, MEM amino acids solution [Gibco; Thermo Fisher, Waltham, MA, USA], MEM vitamin solution [Gibco; Thermo Fisher, Waltham, MA, USA], and 1.5 mg/ml phenol red) containing 4 mM $CaCl_2$, 0 mM $MgCl_2$, 1 μM tetrodotoxin, and 1 mM MNI-caged glutamate aerated with 95% O_2/5% CO_2 at 24–26°C.

Ca^{2+} imaging in single-spines

To measure Ca^{2+} transients in dendritic spines, the Ti: sapphire laser tuned to 1000 nm was used for the excitation of both GCaMP6f and mScarlet. For image acquisition, 128×32 pixels were acquired at 15.6 Hz. To apply glutamate stimulations at single-spines, bath-applied 1 mM MNI-caged glutamates were uncaged by the second Ti: sapphire laser at the wavelength of 720 nm (1 train, 6 ms duration/pulse, 6 mW, measured under an objective lens) near the spine of interest. Since the focal plane of the imaging (1000 nm) and activation (720 nm) lasers were different (0.5–1.0 μm), it was compensated by moving the sample stage along the z-axis (0.8 μm) with piezo stages during the glutamate uncaging. The glutamate uncaging was carried out in the imaging buffer solution containing 4 mM $CaCl_2$, 0 mM $MgCl_2$, 1 μM tetrodotoxin, and 1 mM MNI-caged glutamate aerated with 95% O_2/5% CO_2 at 24–26°C.

For Ca^{2+} influx quantification, the trace of GCaMP6f fluorescence intensity in a stimulated spine (F) was subtracted by the fluorescence intensity in the pre-stimulation frames (F_0), and further divided by F_0 as the following equation. $\Delta F/F_0 = (F - F_0)/ F_0$.

Two-photon paCaMKII uncaging

To uncage paCaMKII in single-spines with two-photon excitation, the second Ti: sapphire laser tuned to 820 nm was used with 30 trains (0.5 Hz, 80 ms duration/pulse, 4 mW) in the spine of interest. Since the focal plane of the imaging (1010 nm) and activation (820 nm) lasers were different (0.5–1.0 μm), it was compensated by moving the sample stage in the z-axis (0.75 μm) with piezo stages during the paCaMKII uncaging. The paCaMKII uncaging was carried out in the imaging buffer solution containing 2 mM $CaCl_2$ and 2 mM $MgCl_2$ aerated with 95% O_2/5% CO_2 at 24–26°C.

Primary neuronal culture and AAV infection

Low-density cultures of dissociated embryonic mouse hippocampal neurons were prepared as described previously (Murakoshi et al., 2017). Briefly, hippocampi were removed from C57BL/6N mice at embryonic day 18 and treated with papain for 10 min at 37°C, followed by gentle trituration. Hippocampal neurons were seeded onto polyethylenimine-coated 3-cm dishes (2 × 105 cells/dish) and cultured in a neurobasal medium (Gibco; Thermo Fisher, Waltham, MA, USA) supplemented with B-27 and 2 mM Glutamax (Gibco; Thermo Fisher, Waltham, MA, USA). Primary neuronal cultures were infected with AAV-ESARE-mScarlet-Flag at the titer of 4.4×106 genome copies/mL and AAV-CaMKII0.4-FHS-paCaMKII-WPRE3 at the titer of 4.7×106 genome copies/ml at DIV 9. After ~65 hours, we applied 10 μM bicuculline to the cultured neurons for 24 hours, followed by a biochemical assay.

Biochemical assay of autophosphorylation

For the paCaMKII autophosphorylation assay in the cultured hippocampal neurons, the neurobasal medium was replaced with the medium containing no bicuculline and incubated for 1 hour in the CO_2 incubator in accordance with the condition of the sLTP experiment. To induce paCaMKII autophosphorylation, the samples were continuously illuminated with a light-emitting diode (M455L2-C1; Thorlabs, Newton, NJ, USA) at 3.82 mW cm^2 for 5 min. The reactions were stopped at the indicated times by adding a lysis solution (50 mM Tris pH 7.5, 1% NP-40, 5% glycerol, 150 mM NaCl, and 4 mM ethylenediaminetetraacetic acid). The samples were collected and centrifuged, and the supernatant was dissolved in sodium dodecyl sulfate sample buffer and analyzed by western blotting.

Western blotting was performed with the following antibodies: anti-phospho-CaMKII (Thr286) (D21E4; Cell Signaling Technology, MA, USA), anti-CaMKIIα (6G9; Cell Signaling Technology, MA, USA), anti-β-Actin (8H10D10; Cell Signaling Technology, MA, USA), anti-CaMKIIβ (ab34703; Abcam), anti-RFP for mScarlet detection (M204-3, MBL; Nagoya, Japan), and horseradish peroxidase-anti-mouse and -rabbit antibodies (Jackson Laboratory, Bar Harbor, ME, USA).

Quantification and statistical analysis

Statistical analyses were performed using MATLAB (Math Works, MA, USA) and GraphPad Prism (GraphPad, SanDiego, CA, USA) software. The types of statistical tests, number of samples, and thresholds for statistical significance are described in the legends.

Results

Homeostatic responses of hippocampal neurons to chronic neuronal excitation

To label neurons excited chronically, we used a synthetic activity-dependent promoter, ESARE, an enhanced version of an activity-regulated cytoskeleton-associated protein (Arc) promoter (Kawashima et al., 2013). The ESARE promoter was combined with a fast-maturation mutant of a yellow fluorescent protein, Achilles, with a destabilization signal, termed d2Achilles (Figure 1A) (Li et al., 1998; Yoshioka-Kobayashi et al., 2020). We injected an AAV encoding ESARE-d2Achilles into the CA1 area of hippocampal slices, and the pyramidal neurons were transfected with the gene construct. After 5–8 days, to induce chronic neuronal excitation, we applied the $GABA_A$ receptor antagonist bicuculline (10 μM) to cultured hippocampal slices for 24 hours (Figure 1B). We successfully observed neurons expressing d2Achilles fluorescence (i.e., chronically-excited neurons) after the bicuculline treatment (Figure 1C). As control experiments, we labeled non-treated neurons by injecting AAV-CaMKII0.4-DIO-Achilles with a low concentration of AAV-hSyn-Cre for sparse expressions of Achilles (Figure 1A). To confirm a neuronal response to the bicuculline treatment, we measured the density of dendritic spines. Previous studies reported the reduction in spine density after neuronal excitation as a homeostatic response for neuronal stability (Fiore et al., 2014; Goold and Nicoll, 2010; Mendez et al., 2018; Moulin et al., 2019). Consistent with the previous studies, the spine density of chronically-excited neurons was significantly decreased compared with that of the non-treated neurons (Figures 1D and 1E), indicating that the bicuculline application for 24 hours induces the homeostatic response of chronically-excited neurons.

Suppression of structural LTP induction in chronically-excited neurons

To investigate metaplastic regulations in the structural plasticity of dendritic spines, we applied a low-frequency train of two-photon glutamate uncaging to single spines (720 nm, 0.5 Hz, 30 pulses, 6 ms duration/pulse, 6 mW) and monitored the change of d2Achilles or Achilles fluorescence within spines as the volume of spine heads using a two-photon microscope at 920 nm (Figures 2A and 2B). In the control experiments, the volume of the stimulated spines, but not adjacent spines, was rapidly expanded (327%, 2–4 min: transient phase) and maintained at a larger level than that before the stimulation (110%, 20–30 min: sustained phase) (Figures 2C and 2D). In contrast, such spine enlargement was not induced in chronically-excited neurons (Figures 2A–2D). We further confirmed the failure of sLTP induction after an application of another $GABA_A$ receptor antagonist, gabazine, for 24 hours (Figure 3). To diminish depth-dependent effects on glutamate uncaging, we chose the target spines located in the range of 10–50 μm from the surface of slices, where the strength of sLTP was not correlated with the depth of glutamate uncaging (Figure 4). These results demonstrate that chronic neuronal excitation leads to the suppression of sLTP in CA1 pyramidal neurons.

Protein synthesis dependency of structural LTP suppression in chronically-excited neurons

Chronic neuronal excitation with bicuculline enhances protein synthesis and degradations (Dorrbaum et al., 2020; Schanzenbacher et al., 2018; Schanzenbacher et al., 2016). It has been reported that protein synthesis is required for homeostatic responses such as a reduction in spine density (Mendez et al., 2010). Thus, we expected that the sLTP suppression also needs protein synthesis. To examine this, we added a protein synthesis inhibitor, anisomycin (100 μM), along with bicuculline to cultured slices for 24 hours (Figure 5A). Since the

anisomycin treatment inhibits the activity-dependent protein synthesis of d2Ahilles, CA1 pyramidal neurons were labeled by injecting AAV-CaMKII0.4-DIO-Achilles with a low concentration of AAV-hSyn-Cre (Figure 5B), instead of AAV-ESARE-d2Achilles. sLTP induction also failed in Achilles-expressing neurons after the bicuculline treatment (Figures 5C–5F). Notably, after the anisomycin with bicuculline treatment, while the spine enlargement in the transient phase was not significantly recovered, the increased spine volume was successfully maintained in the sustained phase at a lower level than that of the non-treated neurons (Figures 5C–5F). This partial effect of anisomycin suggests that the mechanisms of the sLTP suppression partially depend on protein synthesis during chronic neuronal excitation.

Reduction in Ca^{2+} influx into single dendritic spines of chronically-excited neurons

Next, to investigate the molecular mechanisms for sLTP suppression, we focused on Ca^{2+} influx into single-spines induced by glutamate uncaging. Prolonged neuronal excitation reduces postsynaptic NMDAR expressions and currents (Ehlers, 2003; Goold and Nicoll, 2010; Watt et al., 2000). Thus, it is possible that NMDAR-mediated Ca^{2+} influx is decreased in chronically-excited neurons, causing the suppression of sLTP. To evaluate the Ca^{2+} influx, we expressed a genetically-encoded calcium indicator, GCaMP6f, in CA1 pyramidal neurons by the transfection of CMV-GCaMP6f-P2A-mScarlet using a gene gun (Figure 6A) (Bindels et al., 2017; Chen et al., 2013). After the bicuculline treatment, GCaMP6f fluorescence intensity within single-spines during a single pulse of glutamate uncaging (720 nm, 6 ms duration/pulse, 6 mW) was monitored as the strength of Ca^{2+} signals (Figure 6B). We found that the increase of Ca^{2+} signals during glutamate uncaging was suppressed in the bicuculline-treated neurons (Figure 6C). Quantitative analysis revealed that the peak amplitude of Ca^{2+} transients ($\Delta F/F_0$) in the bicuculline-treated neurons was significantly

decreased compared with the non-treated neurons (Figures 6D and 6E). We confirmed that the basal GCaMP6f intensities were comparable (Figure 7). To diminish depth-dependent effects on glutamate uncaging, we chose the target spines located in the range of 4–50 μm from the surface of slices, where the peak amplitude of Ca^{2+} transients did not correlate with the depth of spines (Figure 8).

To address the mechanisms for the Ca^{2+} influx reduction, we measured Ca^{2+} signals in the presence of a GluN2B-containing NMDAR selective antagonist ifenprodil (3 μM) or an NMDAR non-selective antagonist AP5 (100 μM). In the non-treated neurons, AP5 abolished the Ca^{2+} transients (Figure 6E), indicating that glutamate uncaging-evoked Ca^{2+} influx through NMDARs. Also, ifenprodil significantly reduced Ca^{2+} transients (Figure 6E), indicating that GluN2B-containing NMDARs are a major source of glutamate uncaging-evoked Ca^{2+} influx into single-spines. However, in the bicuculline-treated neurons, ifenprodil did not significantly decrease the Ca^{2+} transients, while the effect of AP5 was similar to that of the non-treated neurons (Figure 6E). These results demonstrate that chronic neuronal excitation induces the inhibition of the GluN2B-containing NMDAR-mediated Ca^{2+} influx, leading to the reduction in the glutamate uncaging-evoked Ca^{2+} influx. To exclude contributions of other Ca^{2+} sources to this Ca^{2+} reduction, we measured Ca^{2+} transients in the presence of some inhibitory drugs for Ca^{2+}-permeable AMPARs, metabotropic glutamate receptors (mGluRs), intracellular calcium stores, or voltage-gated calcium channels (VGCCs) (Figure 9). None of them decreased the peak amplitude of Ca^{2+} transients (Figure 9). Since glutamate uncaging-induced sLTP requires the process of NMDAR-mediated Ca^{2+} entries (Matsuzaki et al., 2004), this Ca^{2+} reduction would play a role in the sLTP suppression in chronically-excited neurons.

As mentioned above, the sLTP suppression in chronically-excited neurons partially depends on protein synthesis. However, we found that the inhibition of Ca^{2+} influx through

NMDAR was independent of protein synthesis (Figures 6C–E). This result is consistent with a finding from a previous study wherein postsynaptic NMDAR currents were reduced by chronic neuronal activation via a protein synthesis-independent pathway (Goold and Nicoll, 2010). The difference in protein synthesis dependency between the inhibitions of sLTP and Ca^{2+} influx implies other mechanisms that play a role in sLTP suppression.

Inhibition of CaMKII signaling for structural LTP in chronically-excited neurons

Next, we focused on CaMKII signaling that is downstream from Ca^{2+} influx within the signal cascade for sLTP. It has been demonstrated that the activation of CaMKII signaling is necessary for sLTP induction in hippocampal neurons (Bayer and Schulman, 2019; Giese and Mizuno, 2013; Herring and Nicoll, 2016; Lisman et al., 2012). Thus, it is possible that the chronic excitation induces the inhibition of CaMKII signaling, causing sLTP suppression. To examine this possibility, we applied sLTP inductions by direct activations of CaMKII signaling using paCaMKII (Shibata et al., 2021). paCaMKII is composed of a CaMKIIα subunit and a light-sensitive domain LOV2-Jα that is genetically inserted between the kinase domain and the regulatory domain of CaMKIIα (Figure 10A). paCaMKII proteins form dodecamers with endogenous CaMKII subunits via their association domains in hippocampal neurons. Two-photon excitation at about 820 nm or blue light exposure induces the conformational change of LOV2-Jα, which triggers releases of the kinase domains from the regulatory domain-dependent inhibitions in a reversible manner. The activated paCaMKII phosphorylates CaMKII downstream molecules, leading to sLTP at the spines.

We first examined whether glutamate and paCaMKII uncaging share the signaling for sLTP induction. To this end, we performed occlusion experiments (Figure 11). We co-

injected AAV-tdTomato-P2A-paCaMKII, AAV-CaMKII0.4-DIO-Achilles, and a low concentration of AAV-hSyn-Cre into the CA1 area of cultured slices and identified the injection site by observing tdTomato fluorescence under an epifluorescence microscope (Shaner et al., 2004). Subsequently, CA1 pyramidal neurons expressing Achilles and tdTomato were detected by a two-photon microscope at the excitation wavelength of 1010 nm. We applied paCaMKII uncaging at single-spines (820 nm, 0.5 Hz, 30 pulses, 80 ms duration/pulse, 4 mW) as the first stimulation, followed by the second stimulation of glutamate uncaging (720 nm, 0.5 Hz, 30 pulses, 6 ms duration/pulse, 6 mW). The spine enlargement induced by glutamate uncaging was occluded in both the transient and sustained phases after the paCaMKII-induced sLTP (Figures 11A–11C). The reverse experiment (i.e., glutamate uncaging followed by paCaMKII uncaging) showed the occlusion in the sustained phase but not the transient phase (Figures 11D–11F). This spine expansion in the transient phase may be due to the difference in the signaling for sLTP induction because glutamate uncaging activates other signaling pathways than CaMKII signaling, such as calcineurin, PKC, and PKA (Colgan et al., 2018; Fujii et al., 2013; Oh et al., 2015; Tang and Yasuda, 2017). These results suggest that glutamate and paCaMKII uncaging largely share the signaling for sLTP induction, especially for the sustained phase. Thus, paCaMKII uncaging would activate CaMKII signaling, which is the same pathway as glutamate uncaging, leading to sLTP.

To investigate the contributions of CaMKII signaling to the sLTP suppression, we applied paCaMKII uncaging in single-spines of chronically-excited neurons (Figure 10B). As control experiments, we co-injected AAV-tdTomato-P2A-paCaMKII, AAV-CaMKII0.4-DIO-Achilles, and a low concentration of AAV-hSyn-Cre for the sparse neuronal labeling. paCaMKII uncaging in the non-treated neurons successfully induced the spine enlargement (i.e., sLTP) at the level of approximately 250% in the transient phase (4–

6 min) and 83% in the sustained phase (20–30 min) (Figures 10C–10F). To examine whether paCaMKII uncaging induces sLTP in chronically-excited neurons, we co-injected AAVs encoding tdTomato-P2A-paCaMKII and ESARE-d2Ahilles (Figure 10B) and applied bicuculline for 24 hours. We found that paCaMKII-induced sLTP did not occur in the chronically-excited neurons (Figures 10C–10F). To diminish depth-dependent effects on paCaMKII uncaging, we chose the target spines located in the range of 8–35 μm from the surface of slices, where the strength of sLTP did not largely correlate with the depth of paCaMKII uncaging (Figure 12).

A possible explanation for the failure of paCaMKII-induced sLTP was that the bicuculline treatment might decrease the expression/activity of paCaMKII. To examine this, we assessed the level of expression and activity of paCaMKII using a biochemical assay. Dissociated hippocampal neurons were transfected with CaMKII0.4-paCaMKII and ESARE-mScarlet through the AAVs (Figure 13A) and activated for 24 hours with bicuculline (10 μM). The bicuculline-induced activations were confirmed as the robust expressions of mScarlet under the ESARE promoter (Figure 13B). The expression levels of paCaMKII were consistent under the conditions of the non- and bicuculline-treated neurons (Figure 13B). Furthermore, the blue light-dependent pT286 autophosphorylation of paCaMKII was unaffected by the bicuculline treatment (Figure 13B), indicating that chronic neuronal excitation does not affect the function of paCaMKII. Taken together, the suppression of paCaMKII-induced sLTP is due to the inhibition of the CaMKII downstream signaling rather than the impairment of paCaMKII itself.

A bicuculline application increases the intracellular Ca^{2+} concentration in cultured hippocampal slices (van der Linden et al., 1993). Since the high Ca^{2+} triggers CaMKII signaling, the long-lasting Ca^{2+} elevation during the bicuculline treatment for 24 hours might saturate the activity of CaMKII downstream signaling, resulting in the failure of paCaMKII-

induced sLTP. To test this possibility, we extended the duration per pulse of the two-photon excitation in paCaMKII with the fixed pulse number (320 ms/pulse) (Figure 14A) and examined whether the augmented paCaMKII activation overcomes the sLTP suppression in the chronically-excited neurons. In the non-treated neurons, the prolonged paCaMKII uncaging stimuli elicited larger spine enlargements compared with the control stimuli (80 ms/pulse) (Figures 14B–14D). This enhanced sLTP is most likely due to the increased activity of CaMKII downstream signaling induced by the longer paCaMKII uncaging. Even in the bicuculline-treated neurons, sLTP was successfully elicited by the longer paCaMKII uncaging (Figure 14), indicating that the activity of CaMKII downstream signaling is inhibited rather than saturated by the bicuculline treatment. This inhibitory mechanism within the CaMKII downstream signaling for sLTP would raise the threshold for sLTP induction.

Finally, we examined whether the inhibition of the CaMKII downstream depends on newly-protein synthesis. We injected AAV-tdTomato-P2A-paCaMKII, AAV-CaMKII0.4-DIO-Achilles, and a low amount of AAV-CaMKII0.4-Cre and added anisomycin to the bicuculline treatment. While paCaMKII-induced sLTP was suppressed in the bicuculline-treated neurons, the anisomycin treatment completely recovered the spine enlargement in both the transient and sustained phases (Figure 15). This finding indicates that the inhibition of the CaMKII downstream signaling for sLTP is mediated by the protein synthesis during the chronic excitation and that this is an independent mechanism from the inhibition of Ca^{2+} influx due to the difference in protein synthesis dependency.

Discussion

In this study, we demonstrate that sLTP induction is suppressed in chronically-excited hippocampal neurons and revealed molecular mechanisms for the metaplastic regulation of sLTP (Figure 16). The two inhibitory mechanisms (i.e., the inhibitions of GluN2B-containing NMDAR-mediated Ca^{2+} influx and CaMKII downstream signaling) decrease the probability of sLTP induction at single dendritic spines. While the reduction in Ca^{2+} influx is independent of newly-protein synthesis induced by chronic excitation, the inhibition of CaMKII downstream requires it. This two-layered inhibition in the signaling for sLTP leads to the robust suppression of sLTP and maintains homeostasis of neuronal excitability.

One proposed mechanism for metaplasticity has been the composition change of NMDAR subunits in postsynapses (Perez-Otano and Ehlers, 2005; Shipton and Paulsen, 2014; Yashiro and Philpot, 2008). For example, it has been demonstrated that chronic silencing at single-synapses increases the GluN2B subunit composition and Ca^{2+} influx induced by glutamate uncaging, which in turn decreases the threshold for LTP induction (Lee et al., 2010). In the condition of chronic excitation, however, the change of NMDAR-mediated Ca^{2+} influx into single-spines had been unclear. Here, we found the reduction in glutamate uncaging-induced Ca^{2+} influx into single-spines of chronically-excited neurons. Pharmacological experiments uncovered that the Ca^{2+} reduction is caused by the decrease in GluN2B-containing NMDAR-mediated Ca^{2+} influx. This result is consistent with previous studies showing the down-regulation of postsynaptic GluN2B subunits after prolonged neuronal excitation (Ehlers, 2003).

We found that the reduction in NMDAR-mediated Ca^{2+} influx is induced in a protein synthesis-independent manner. This mechanism is consistent with the evidence that chronic optogenetic activation of hippocampal neurons leads to depressions of postsynaptic

NMDAR currents via a protein synthesis-independent pathway (Goold and Nicoll, 2010). The precise mechanism that induces the down-regulations of postsynaptic NMDARs remains unclear. Activity-dependent cellular processes, such as endocytosis (Snyder et al., 2001) and protein degradation (Ehlers, 2003), may contribute to postsynaptic NMDAR down-regulation (Perez-Otano and Ehlers, 2005).

The NMDAR-based mechanism for metaplasticity has been investigated (Barria and Malinow, 2005; Berberich et al., 2005; Bridi et al., 2018; Morishita et al., 2007; Philpot et al., 2007; Philpot et al., 2001; Quinlan et al., 1999; Tang et al., 1999), However, it had been unknown whether the downstream molecules are involved in the metaplastic regulation of sLTP induction. Here, we applied the direct activation of CaMKII signaling at single-spines using paCaMKII uncaging and found that paCaMKII uncaging failed to induce sLTP after the bicuculline treatment, demonstrating that the CaMKII signaling for sLTP is inhibited in chronically-excited neurons. The expression and photo-sensitivity of paCaMKII were unaffected by the chronic excitation, suggesting that inhibitions of the CaMKII downstream signaling cause the paCaMKII-induced sLTP suppression. This inhibitory mechanism contributes to the elevation of the sLTP threshold because the augmented paCaMKII activation successfully induced sLTP in the chronically-excited neurons.

Notably, the suppression of paCaMKII-induced sLTP requires protein synthesis processes during the bicuculline treatment. Thus, it is possible that chronic excitation-dependent newly-synthesized proteins induce the metaplastic regulation in the CaMKII downstream signaling for sLTP. Indeed, prolonged applications of bicuculline enhance expressions of numerous proteins in cultured hippocampal neurons (Schanzenbacher et al., 2018; Schanzenbacher et al., 2016). Some of these proteins are known to contribute to neuronal homeostasis by changing the property of dendritic spines. For example, Arc proteins are accumulated in spines and elicit internalizations of the surface AMPARs and reductions in

the spine size (Okuno et al., 2012; Peebles et al., 2010; Shepherd et al., 2006). Homer1a also has the similar effects that induce the down-regulations of postsynaptic AMPARs and morphologies (Diering et al., 2017; Hu et al., 2010; Sala et al., 2003). Thus, these proteins can suppress the spine enlargement induced by the activation of CaMKII downstream in chronically-excited neurons. Plk2 and Nr4a1 are also expressed in response to neuronal excitation (Chen et al., 2014; Fiore et al., 2014; Lee et al., 2011; Seeburg and Sheng, 2008). These proteins inhibit small GTPases signaling, such as Ras and Rac1, by modulating guanine nucleotide exchange factors (GEFs)/GTPase activating proteins (GAPs), leading to the reduction in the spine density and head width. The Ras and Rac1 are downstream molecules of CaMKII and are associated with sLTP induction (Araki et al., 2015; Harvey et al., 2008; Hedrick et al., 2016; Saneyoshi et al., 2019). Intriguingly, these activated small GTPases lower the sLTP threshold in neighboring spines of the sLTP-expressing spine (Harvey and Svoboda, 2007; Hedrick et al., 2016). Therefore, it is presumed that Plk2 and Nr4a1 expressions can decrease the activity of the small GTPases in the CaMKII downstream, resulting in the elevation of the sLTP threshold in chronically-excited neurons.

Based on the findings in this study, we propose that the inhibition of CaMKII downstream signaling, in combination with the reduction in NMDAR-Ca^{2+} signals, is a mechanism for metaplastic regulation of sLTP in chronically-excited neurons. This dual inhibitory mechanism in the signaling for sLTP can provide the robust suppression of runway sLTP induction and maintain spine stability in excitable environments.

Acknowledgments

I would like to express my deepest appreciation to Professor Hideji Murakoshi for his patience and excellent support from the first day I joined his lab until the present. Thanks to his constant guidance, I could accomplish this research and write these.

I am extremely grateful to Dr. Akihiro Shibata, who taught me two-photo microscope methods. I would like to thank Mr. Yutaro Nagasawa for performing additional experiments during the revision process of this paper. I also would like to thank Ms. Aiko Sato, Ms. Maki Onda, and Ms. Kayo Hirata for their technical assistance with experiments.

I sincerely appreciate all members of the Division of Homeostatic Development in the National Institute of Physiological Sciences for helpful advice on this study in the progress meeting.

Figures and Figure Legends

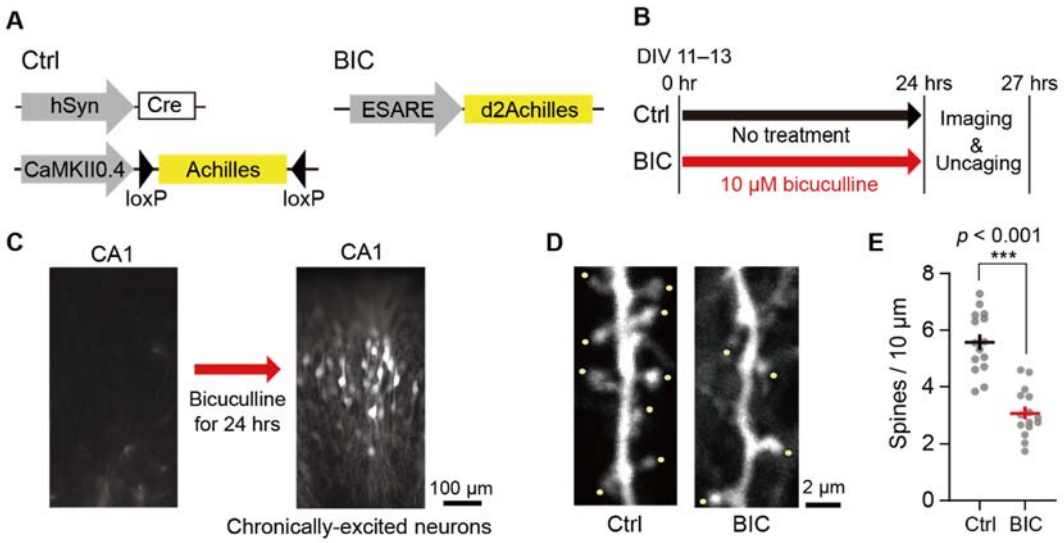

Figure 1. Chronic application of bicuculline-induced neuronal activations and decreased the spine density of CA1 pyramidal neurons in cultured hippocampal slices.
(A) In the control experiments (Ctrl), AAVs encoding Cre under human synapsin promoter (Syn) and Achilles double-floxed inverse orientation (DIO) under the 0.4 kb version of CaMKII promoter (CaMKII0.4) were used for sparse labeling. For the group treated with bicuculline (BIC), AAV encoding d2Achilles under the activity-dependent promoter ESARE was used to label the chronically-excited neurons.
(B) Schematic timelines for the experiments of two-photon imaging and glutamate uncaging. To chronically excite neurons, hippocampal slices were incubated in a culture medium containing bicuculline (BIC) for 24 hours. Subsequently, the slices were placed in an imaging buffer, and the experiments were carried out for up to 3 hours.

(C) Epifluorescence images of cultured hippocampal slices transfected with ESARE-d2Achilles. No d2Achilles expression was observed before the bicuculline treatment. After the treatment, several CA1 pyramidal neurons expressed d2Achilles fluorescence.
(D and E) Measurement of spine densities in the CA1 pyramidal neurons. Yellow points indicate counted spines. The number of samples (dendrites/neurons) was 15/5 for Ctrl and 15/5 for BIC, respectively. The data are presented as mean ± SEM. Statistical comparisons were performed using a two-tailed unpaired t-test. ***$p < 0.001$.

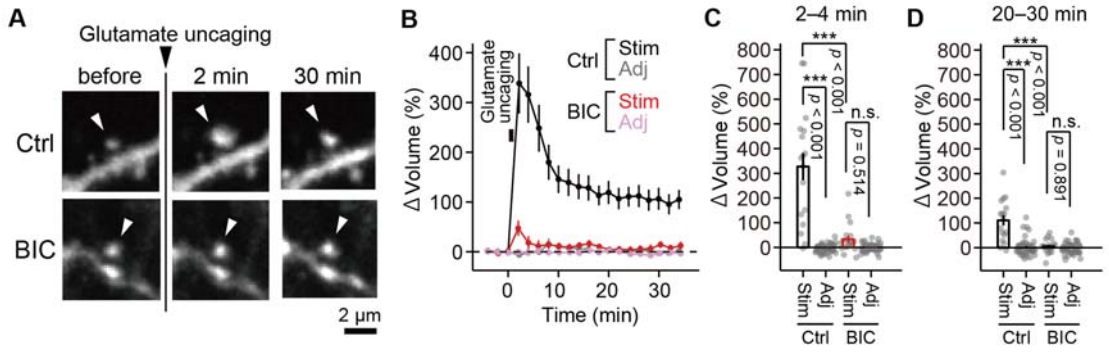

Figure 2. sLTP induced by glutamate uncaging was suppressed after the bicuculline treatment.

(A) Two-photon fluorescence images of dendritic spines during sLTP induction by glutamate uncaging. CA1 pyramidal neurons expressing Achilles or d2Achilles were observed by two-photon excitation at 920 nm, and MNI-glutamates were uncaged at 720 nm (30 trains, 0.5 Hz, 6 ms duration/pulse, 6 mW) on a spine indicated by white arrows.

(B) Averaged time courses of the changes in spine volume upon glutamate uncaging in the stimulated (BIC-Stim) and adjacent spines (2–10 μm, BIC-Adj) after the bicuculline treatment. For comparison, a time course of the stimulated spines (Ctrl-Stim) and adjacent spines (2–10 μm, Ctrl-Adj) that were not treated with bicuculline is also shown. The number of samples (spines/neurons) was 17/9 for Ctrl-Stim, 47/9 for Ctrl-Adj, 19/9 for BIC-Stim, and 45/9 for BIC-Adj. Approximately half of the experiment was done in blind experiments.

(C and D) Quantification of the transient (C, averaged over 2–4 min) and sustained (D, averaged over 20–30 min) changes in spine volume. The data are presented as mean ±SEM. Statistical comparisons were performed using one-way analysis of variance followed by Turkey's test. ***$p < 0.001$; n.s. represents $p > 0.05$.

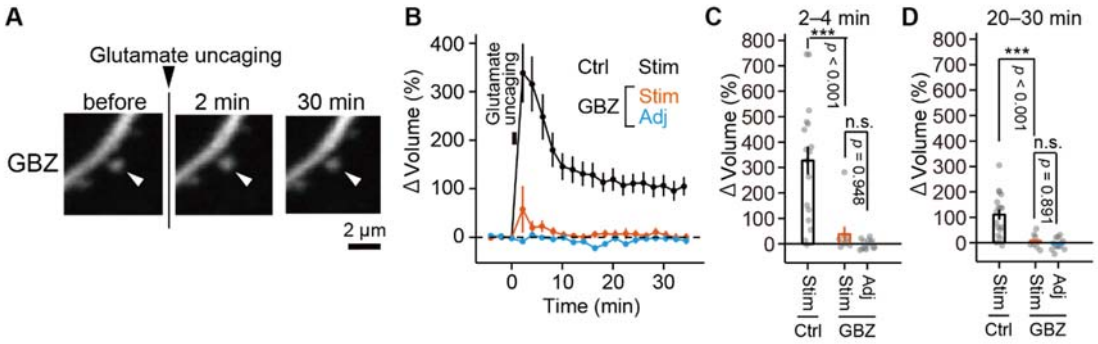

Figure 3. sLTP induced by glutamate uncaging was suppressed after a chronic application of gabazine.

(A) Two-photon fluorescence images of dendritic spines during sLTP induction by glutamate uncaging. CA1 pyramidal neurons expressing d2Achilles were observed by two-photon excitation at 920 nm, and MNI-glutamates were uncaged at 720 nm (30 trains, 0.5 Hz, 6 ms duration/pulse, 6 mW) on a spine indicated by white arrows.

(B) Averaged time courses of the change in spine volume upon glutamate uncaging in the stimulated (GBZ-Stim) and adjacent spines (2–10 μm, GBZ-Adj) after the gabazine treatment. For comparison, the time course of the stimulated spines (Ctrl-Stim used in Fig. 2B) is replotted. The number of samples (spines/neurons) was 10/4 for GBZ-Stim, and 13/4 for GBZ-Adj.

(C and D) Quantification of the transient (C, averaged over 2–4 min) and sustained (D, averaged over 20–30 min) changes in spine volume. The data are presented as mean ± SEM. Statistical comparisons were performed using one-way analysis of variance followed by Tukey's test. ***$p < 0.001$; n.s. represents $p > 0.05$.

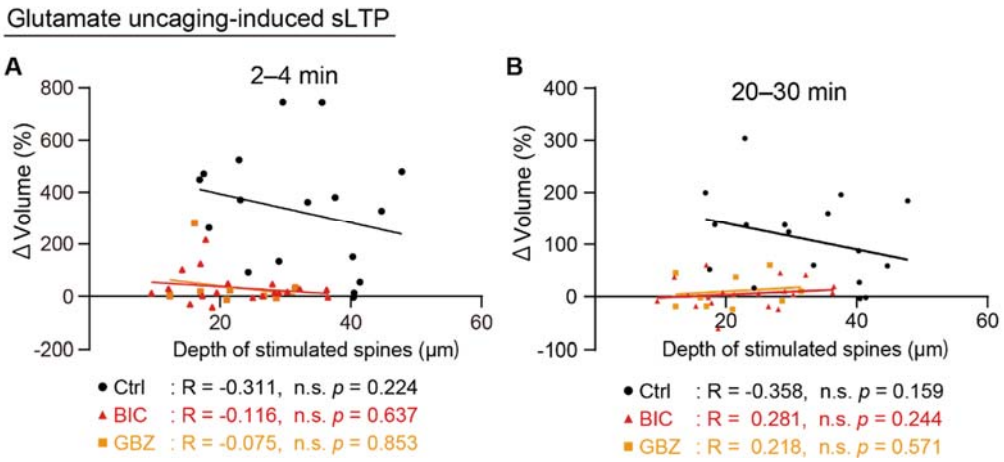

Figure 4. The changes in spine volume induced by glutamate uncaging were uncorrelated with the depths of the stimulated spines.

(A and B) The spine volume changes were plotted against the depths of glutamate uncaging in hippocampal cultured slices. The same data set used in Figures 2 and 3 was analyzed [non- (Ctrl), bicuculline (BIC), gabazine (GBZ) treatments]. The volume changes were quantified in the transient (A, averaged over 2–4 min) and sustained phases (B, averaged over 20–30 min).

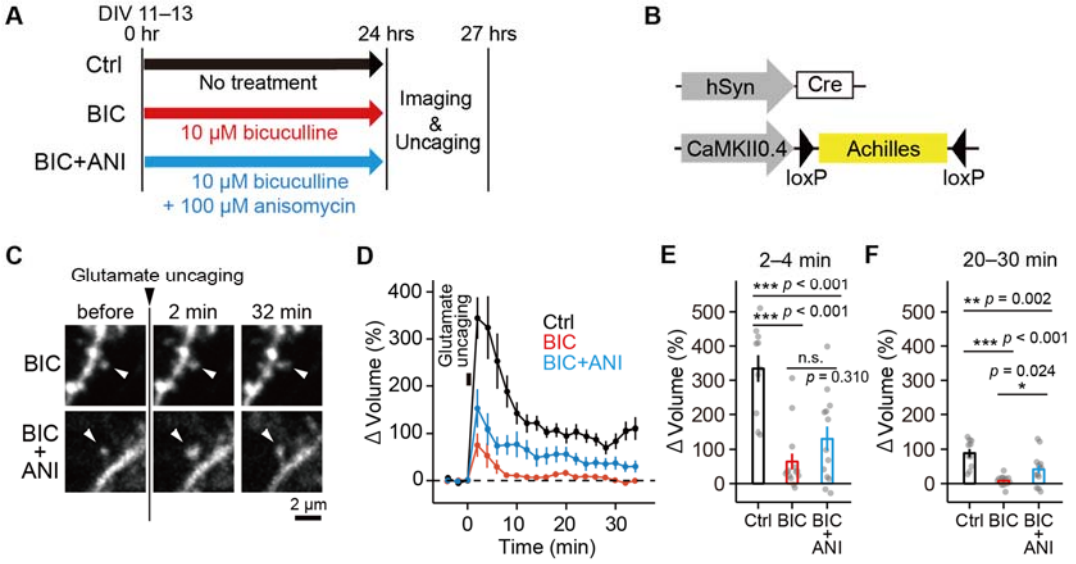

Figure 5. The suppression of glutamate uncaging-induced sLTP partially depended on protein synthesis during chronic neuronal excitation.

(A) Schematic timelines for the experiments of control (Ctrl), bicuculline treatment (BIC), and anisomycin with bicuculline treatment (BIC+ANI).

(B) Schematics of AAV-hSyn-Cre and AAV-CaMKII0.4-DIO-Achilles used in the experiments.

(C) Two-photon fluorescence images of dendritic spines during the induction of sLTP by two-photon glutamate uncaging. CA1 pyramidal neurons expressing Achilles were observed by two-photon excitation at 920 nm, and caged glutamates were uncaged at 720 nm (30 trains, 0.5 Hz, 6 ms duration/pulse, 6 mW) on a spine indicated by white arrows.

(D) Averaged time courses of the volume changes in stimulated spines upon glutamate uncaging in the Ctrl, BIC, and BIC+ANI conditions. The number of samples (spines/neurons) was 10/7 for Ctrl, 14/7 for BIC, and 13/5 for BIC+ANI.

(E and F) Quantification of the transient (E, averaged over 2–4 min) and sustained (F, averaged over 20–30 min) changes in spine volume. The data are presented as mean ± SEM. Statistical comparisons were performed using one-way analysis of variance followed by Tukey's test. ***$p < 0.001$; **$p < 0.01$; *$p < 0.05$; n.s. represents $p > 0.05$.

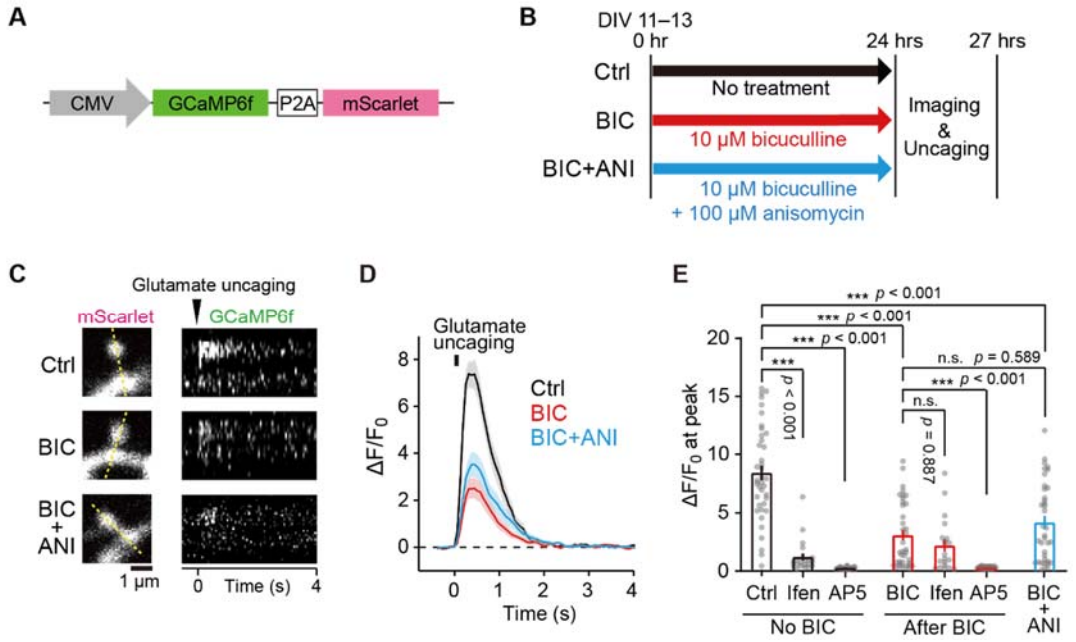

Figure 6. Ca^{2+} influx into single-spines induced by glutamate uncaging was decreased in chronically-excited neurons.

(A) A schematic of CMV-GCaMP6f-P2A-mScarlet transfected into pyramidal CA1 neurons.

(B) Schematic timelines of control (Ctrl), bicuculline (BIC), and anisomycin with bicuculline (BIC+ANI) treatments.

(C) Two-photon fluorescence images of the spines (mScarlet) before glutamate uncaging (left column) and GCaMP6f fluorescence of Ca^{2+} transients in the spines during uncaging (right column) that are shown as kymographs of the yellow dash lines. Both mScarlet and GCaMP6f were imaged by two-photon excitation at 1000 nm, and caged glutamates were uncaged at 720 nm (single pulse, 6 ms duration, 6 mW) at the tip of the spines.

(D) Averaged time courses of Ca^{2+} transients ($\Delta F/F_0$) within the stimulated spines in Ctrl, BIC and BIC+ANI.

(E) Quantification of the peak changes of Ca^{2+} transients ($\Delta F/F_0$) in the absence and presence of ifenprodil 3 μM (Ifen) or AP5 100 μM (AP5). The number of samples (spines/neurons) was 39/10 for Ctrl, 22/5 for Ifen, and 20/5 for AP5 after No BIC; 38/11 for BIC, 20/5 for Ifen, 29/7 for AP5 after BIC; 37/9 for BIC+ANI. The data are presented as mean ± SEM. Statistical comparisons were performed using one-way analysis of variance followed by Tukey's test. ***$p < 0.001$; n.s. represents $p > 0.05$.

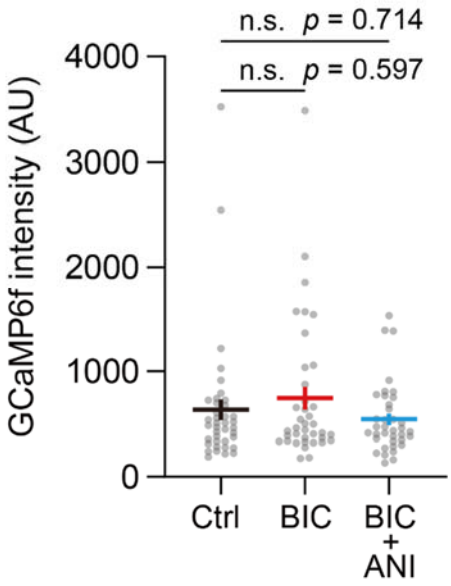

Figure 7. The basal GCaMP6f intensities in single-spines were unchanged after the bicuculline nor anisomycin with bicuculline treatments.

Quantification of the basal GCaMP6f intensities in single-spines in the non- (Ctrl), bicuculline (BIC), and anisomycin with bicuculline (BIC+ANI) treated neurons. The same data set used in Figure 6 was analyzed.

The data are presented as the mean ± SEM. Statistical comparisons were performed using one-way analysis of variance followed by Dunnet's test. n.s. represents $p > 0.05$.

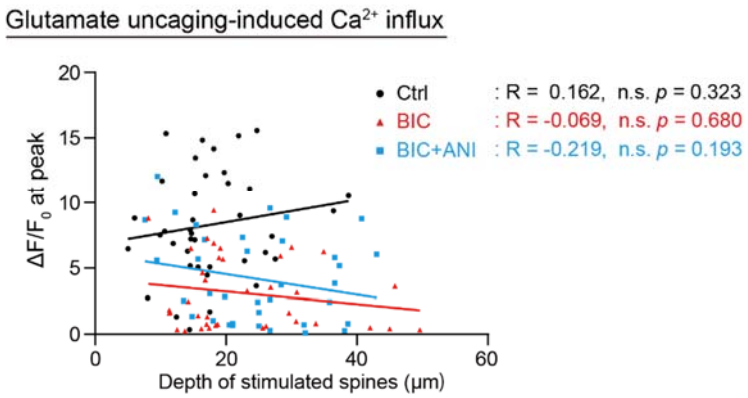

Figure 8. The peak amplitudes of Ca^{2+} influx were uncorrelated with the depths of the stimulated spines.

The peak amplitudes of Ca2+ transients ($\Delta F/F_0$) were plotted against the depths of glutamate uncaging. The same data set used in Figure 6 was analyzed [non- (Ctrl), bicuculline (BIC), anisomycin with bicuculline (BIC+ANI) treatment].

Statistical tests were performed using Spearman's rank correlation. The values of R show Spearman's correlation coefficient. n.s. represents $p > 0.05$.

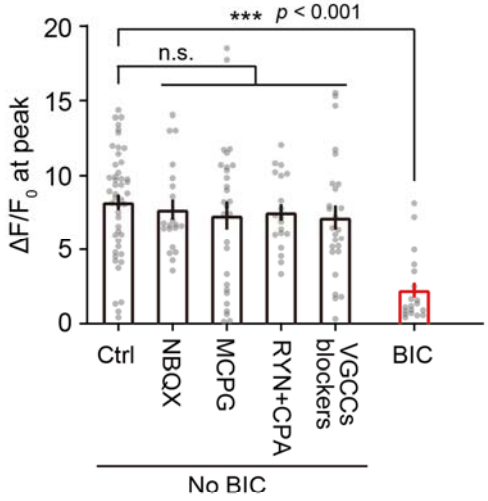

NBQX: AMPA/kainate receptor antagonist

MCPG: Group I /II metabotropic glutamate receptor antagonist

RYN+CPA: Ryanodine (micromolar concentrations are inhibitory) and cyclopiazonic acid (Ca^{2+}-ATPase inhibitor) for blocking CICR (calcium-induced calcium release)

VGCCs blockers: Cocktail of $NiCl_2$, nifedipine, ω-conotoxin GVIA, and ω-agatoxin IVA for blocking R/T-, L-, N-, P-type VGCCs, respectively

Figure 9. No contribution of other Ca^{2+} sources than NMDARs to the reduction in Ca^{2+} influx.

(A) Quantification of Ca^{2+} transients ($\Delta F/F_0$ at peak). The experimental protocol is the same used in Figure 6 without bicuculline treatment (No BIC). Glutamate uncaging was carried out in the absence (Ctrl) and presence of 10 µM NBQX (NBQX), 500 µM MCPG (MCPG), 20 µM ryanodine/ 30 µM cyclopiazonic acid (RYN+CPA), or 50 µM NiCl2/ 10 µM nifedipine/ 100 nM ω-conotoxin GVIA/ 100 nM ω-agatoxin IVA (VGCCs blockers). The number of samples (spines/neurons) was 47/15 for Ctrl, 20/5 for NBQX, 28/7 for MCPG, 20/5 for RYN+CPA, and 26/6 for VGCCs blockers.

The data are presented as mean ± SEM. Statistical comparisons were performed using one-way analysis of variance followed by Dunnet's test. ***$p < 0.001$; n.s. represents $p > 0.05$.

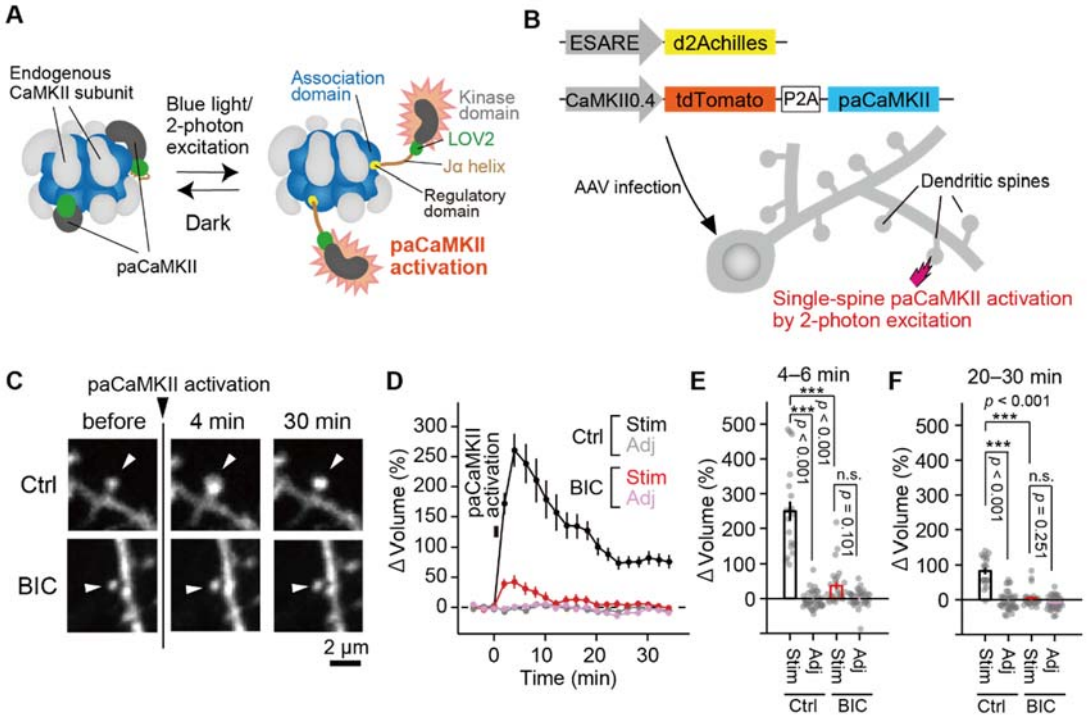

Figure 10. sLTP induced by paCaMKII uncaging was suppressed in chronically-excited neurons.

(A) Schematics drawing of paCaMKII uncaging in the oligomeric state. Two-photon excitation induces structural changes of paCaMKII, thereby activating it. Note that paCaMKII can be integrated into an endogenous CaMKII oligomer. The figure was adopted from a previous paper (Shibata et al., 2021).

(B) A schematic representation of sLTP induction by paCaMKII activation. AAVs encoding CaMKII0.4-tdTomato-P2A-paCaMKII and ESARE-d2Achilles were co-transfected into CA1 pyramidal neurons.

(C) Two-photon fluorescence images of dendritic spines during the induction of sLTP by two-photon paCaMKII uncaging. CA1 pyramidal neurons expressing Achilles or d2Achilles and tdTomato-P2A-paCaMKII were observed by two-photon excitation at 1010 nm, and paCaMKII was uncaged at 820 nm (30 trains, 0.5 Hz, 80 ms duration/pulse, 4 mW) in the spine indicated by white arrows.

(D) Averaged time course of the change in spine volume in the stimulated spine (BIC-Stim) and adjacent spines (2–10 μm, BIC-Adj) after the bicuculline treatment. A control experiment (Ctrl-Stim) and adjacent spines (2–10 μm, Ctrl-Adj) are also shown. The number of samples (spines/neurons) was 19/7 for Ctrl-Stim, 40/7 for Ctrl-Adj, 26/9 for BIC-

Stim, and 35/9 for BIC-Adj. Approximately half of the experiment was done in blind experiments.

(E and F) Quantification of the transient (E, averaged over 4–6 min) and sustained (F, averaged over 20–30 min) changes in spine volume. Data are presented as the mean ± SEM. Statistical comparisons were performed using one-way analysis of variance followed by Tukey's test. ***$p < 0.001$; n.s. represents $p > 0.05$.

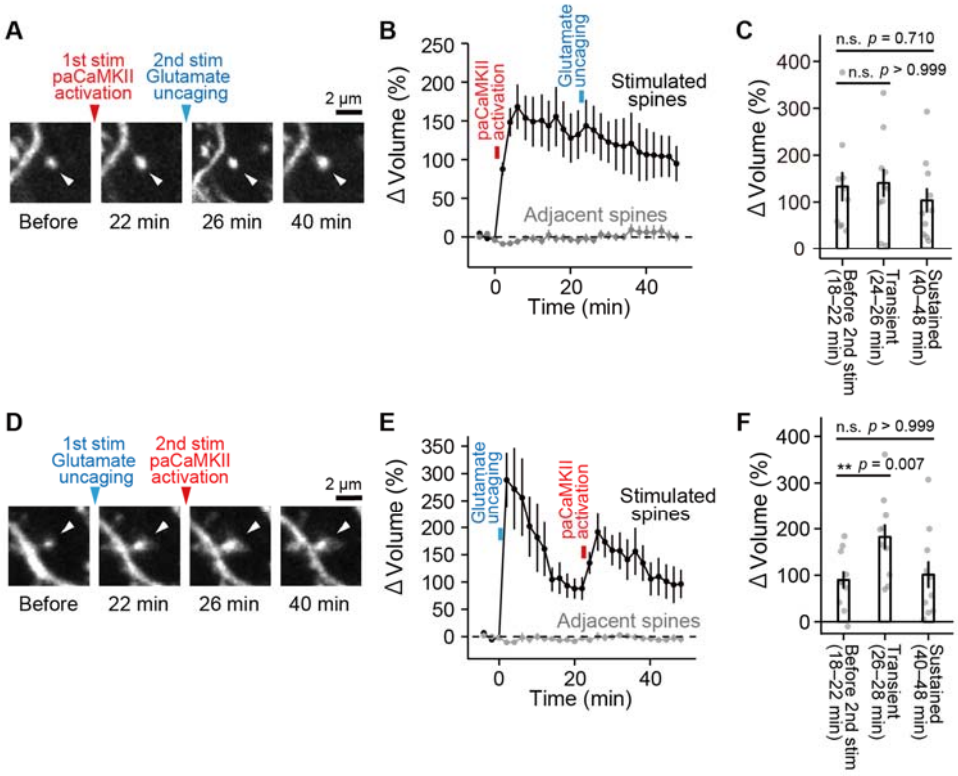

Figure 11. The signaling for sLTP induction was shared between glutamate and paCaMKII uncaging.

(A and D) Two-photon fluorescence images of dendritic spines during the induction of sLTP by two-photon glutamate and paCaMKII uncaging. AAV-CaMKII0.4-tdTomato-P2A-paCaMKII, AAV-CaMKII0.4-DIO-Achilles, and a low concentration of hSyn-Cre were co-infected into CA1 pyramidal neurons. Achilles fluorescence was observed by two-photon excitation at 1010 nm, MNI-glutamate was uncaged at 720 nm (30 trains, 0.5 Hz, 6 ms duration/pulse, 6 mW) and paCaMKII was uncaged at 820 nm (30 trains, 0.5 Hz, 80 ms duration/pulse, 4 mW) on a spine indicated by white arrows. The second stimulation (2nd stim) was applied 22 min after the first stimulation (1st stim) at the same spine.

(B and E) Averaged time courses of spine volume change after 1st or 2nd stimulation. The number of samples (spines/neurons) was 10/7 for (B) and 10/6 for (E).

(C and F) Quantification of spine volume changes after 1st stimulation and in the transient and sustained phases after 2nd stimulation. The data are presented as mean ± SEM of the mean. Statistical comparisons were performed using Friedman's test. **p < 0.01; n.s. represents p > 0.05.

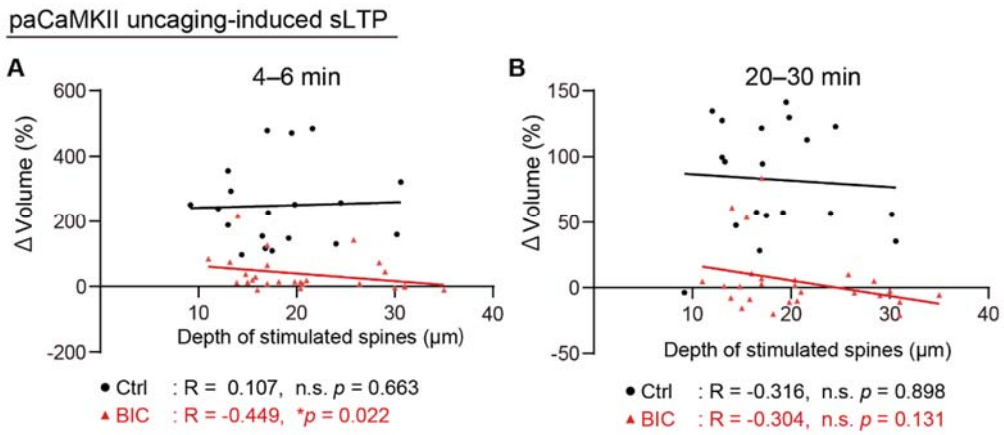

Figure 12. The changes in spine volume induced by paCaMKII uncaging were uncorrelated with the depths of the stimulated spines.

(A and B) The spine volume changes were plotted against the depths of paCaMKII uncaging in hippocampal cultured slices. The same data set used in Figure 10 was analyzed [non-(Ctrl), bicuculline (BIC) treatment]. The volume changes were quantified in the transient (A, averaged over 4–6 min) and sustained phases (B, averaged over 20–30 min).

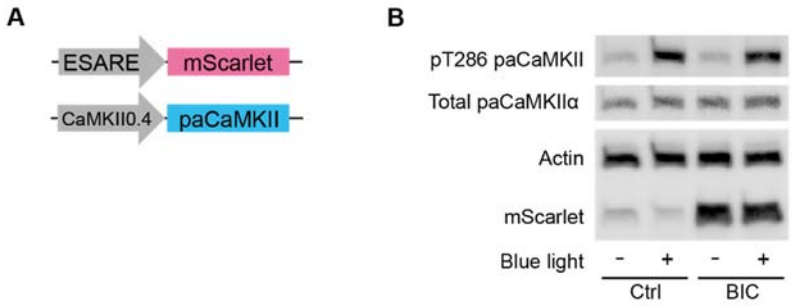

Figure 13. The function and expression of paCaMKII were unchanged after the bicuculline treatment.

(A) Schematics of AAVs encoding ESARE-mScarlet and CaMKII0.4-paCaMKII transfected into neurons for biochemical assays.

(B) Dissociated hippocampal neurons expressing paCaMKII were illuminated with blue light for 5 min after the bicuculline treatment (lane 1: no bicuculline/no light; lane 2: no bicuculline/with light; lane 3: bicuculline/no light; lane 4: bicuculline/with light). The kinase activity and the expression of paCaMKII, actin proteins, and mScarlet were evaluated by western blotting.

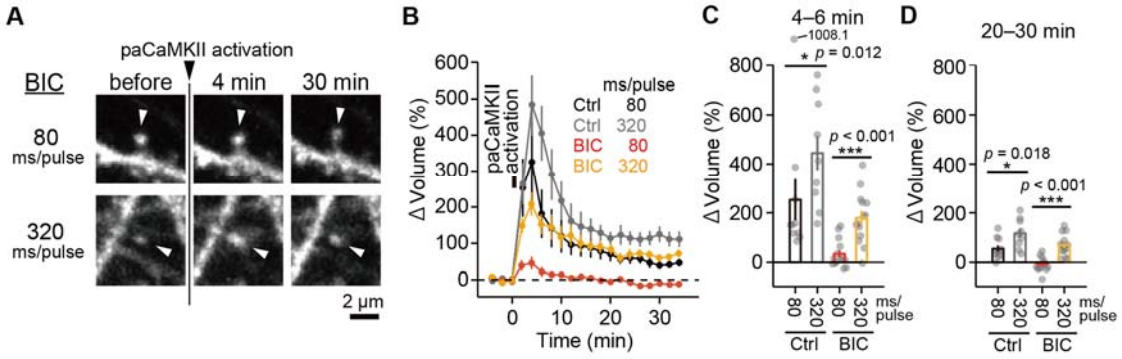

Figure 14. The activity of the CaMKII downstream signaling for sLTP was not saturated in chronically-excited neurons.

(A) Two-photon fluorescence images of dendritic spines during the induction of sLTP by two-photon paCaMKII uncaging after the bicuculline treatment. CA1 pyramidal neurons expressing Achilles or d2Achilles and tdTomato-P2A-paCaMKII were observed by two-photon excitation at 1010 nm, and paCaMKII was uncaged at 820 nm (30 trains, 0.5 Hz, 80 ms or 320 ms duration/pulse, 4 mW) in a spine indicated by white arrows.

(B) Averaged time courses of the changes in spine volume after paCaMKII uncaging with different pulse durations (80 or 320 ms/pulse) are plotted for both the control (Ctrl) and bicuculline-treated neurons (BIC). The number of samples (spines/neurons) was 10/5 for Ctrl with 80 ms/pulse, 9/3 for Ctrl with 320 ms/pulse, 14/5 for BIC with 80 ms/pulse, and 14/5 for BIC with 320 ms/pulse.

(C and D) Quantification of the transient (C, averaged over 4–6 min) and sustained (D, averaged over 20–30 min) phases in spine volume. The data are presented as mean ± SEM. Statistical comparisons were performed using one-way analysis of variance followed by Tukey's test. ***$p < 0.001$; *$p < 0.05$.

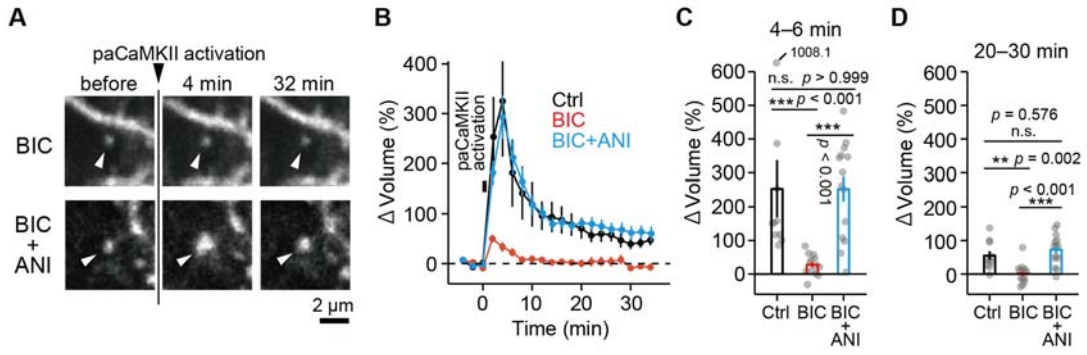

Figure 15. The suppression of paCaMKII uncaging-induced sLTP depended on protein synthesis during chronic neuronal excitation.

(A) Two-photon fluorescence images of dendritic spines during the induction of sLTP by two-photon paCaMKII uncaging. CA1 pyramidal neurons expressing Achilles and tdTomato-P2A-paCaMKII were observed by two-photon excitation at 1010 nm, and paCaMKII was uncaged at 820 nm (30 trains, 0.5 Hz, 80 ms duration/pulse, 4 mW) in a spine indicated by white arrows.

(B) Averaged time courses of the changes in spine volume upon paCaMKII uncaging after the bicuculline (BIC) or anisomycin with bicuculline (BIC+ANI) treatment. For comparison, the averaged time course of the control experiment (no bicuculline/anisomycin treatment Ctrl-Stim in Figure 14B) is also replotted (Ctrl). The number of samples (spines/neurons) was 10/5 for Ctrl, 13/4 for BIC, and 14/5 for BIC+ANI.

(C and D) Quantification of the transient (C, averaged over 4–6 min) and sustained (D, averaged over 20–30 min) phases in spine volume. The data are presented as mean ± SEM. Statistical comparisons were performed using one-way analysis of variance followed by Tukey's test. ***p < 0.001; **p < 0.01; n.s. represents p > 0.05.

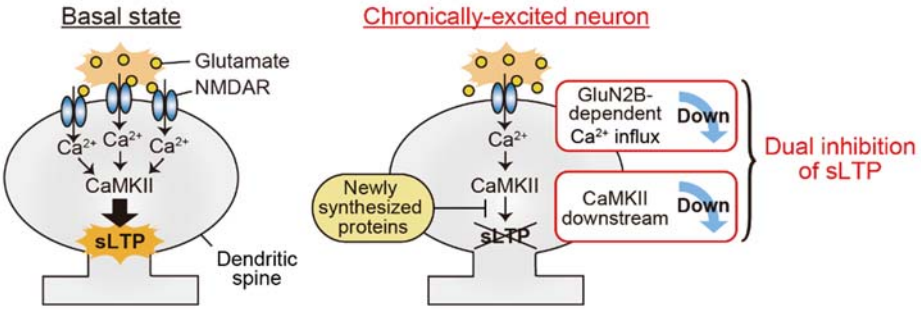

Figure 16. A dual inhibitory mechanism for metaplasticity

In basal states, glutamate stimulation triggers NMDAR-mediated Ca^{2+} influx and activate CaMKII, which thereby induces sLTP at dendritic spines. In chronically-excited neurons, GluN2B-containing NMDAR-mediated Ca^{2+} influx and CaMKII downstream are inhibited in protein synthesis-independent and dependent manners, respectively. This dual inhibition suppresses sLTP induction and provides the metaplastic regulation that decreases the probability of sLTP in hyper-excited neuronal circuits.

References

Abbott, L.F., and Nelson, S.B. (2000). Synaptic plasticity: taming the beast. Nat Neurosci *3 Suppl*, 1178-1183.

Abegg, M.H., Savic, N., Ehrengruber, M.U., McKinney, R.A., and Gahwiler, B.H. (2004). Epileptiform activity in rat hippocampus strengthens excitatory synapses. J Physiol *554*, 439-448.

Abraham, W.C. (2008). Metaplasticity: tuning synapses and networks for plasticity. Nat Rev Neurosci *9*, 387.

Araki, Y., Zeng, M., Zhang, M., and Huganir, R.L. (2015). Rapid dispersion of SynGAP from synaptic spines triggers AMPA receptor insertion and spine enlargement during LTP. Neuron *85*, 173-189.

Arendt, K.L., Sarti, F., and Chen, L. (2013). Chronic inactivation of a neural circuit enhances LTP by inducing silent synapse formation. J Neurosci *33*, 2087-2096.

Barria, A., and Malinow, R. (2005). NMDA receptor subunit composition controls synaptic plasticity by regulating binding to CaMKII. Neuron *48*, 289-301.

Bayer, K.U., De Koninck, P., Leonard, A.S., Hell, J.W., and Schulman, H. (2001). Interaction with the NMDA receptor locks CaMKII in an active conformation. Nature *411*, 801-805.

Bayer, K.U., LeBel, E., McDonald, G.L., O'Leary, H., Schulman, H., and De Koninck, P. (2006). Transition from reversible to persistent binding of CaMKII to postsynaptic sites and NR2B. J Neurosci *26*, 1164-1174.

Bayer, K.U., and Schulman, H. (2019). CaM Kinase: Still Inspiring at 40. Neuron *103*, 380-394.

Berberich, S., Punnakkal, P., Jensen, V., Pawlak, V., Seeburg, P.H., Hvalby, O., and Kohr, G. (2005). Lack of NMDA receptor subtype selectivity for hippocampal long-term potentiation. J Neurosci *25*, 6907-6910.

Bindels, D.S., Haarbosch, L., van Weeren, L., Postma, M., Wiese, K.E., Mastop, M., Aumonier, S., Gotthard, G., Royant, A., Hink, M.A.*, et al.* (2017). mScarlet: a bright monomeric red fluorescent protein for cellular imaging. Nat Methods *14*, 53-56.

Bridi, M.C.D., de Pasquale, R., Lantz, C.L., Gu, Y., Borrell, A., Choi, S.Y., He, K., Tran, T., Hong, S.Z., Dykman, A.*, et al.* (2018). Two distinct mechanisms for experience-dependent homeostasis. Nat Neurosci *21*, 843-850.

Chen, T.W., Wardill, T.J., Sun, Y., Pulver, S.R., Renninger, S.L., Baohan, A., Schreiter, E.R., Kerr, R.A., Orger, M.B., Jayaraman, V.*, et al.* (2013). Ultrasensitive fluorescent proteins for imaging neuronal activity. Nature *499*, 295-300.

Chen, Y., Wang, Y., Erturk, A., Kallop, D., Jiang, Z., Weimer, R.M., Kaminker, J., and Sheng, M. (2014). Activity-induced Nr4a1 regulates spine density and distribution pattern of excitatory synapses in pyramidal neurons. Neuron *83*, 431-443.

Colgan, L.A., Hu, M., Misler, J.A., Parra-Bueno, P., Moran, C.M., Leitges, M., and Yasuda, R. (2018). PKCalpha integrates spatiotemporally distinct Ca(2+) and autocrine BDNF signaling to facilitate synaptic plasticity. Nat Neurosci *21*, 1027-1037.

Cooper, L.N., and Bear, M.F. (2012). The BCM theory of synapse modification at 30: interaction of theory with experiment. Nat Rev Neurosci *13*, 798-810.

Cull-Candy, S.G., and Leszkiewicz, D.N. (2004). Role of distinct NMDA receptor subtypes at central synapses. Sci STKE *2004*, re16.

Derkach, V.A., Oh, M.C., Guire, E.S., and Soderling, T.R. (2007). Regulatory mechanisms of AMPA receptors in synaptic plasticity. Nat Rev Neurosci *8*, 101-113.

Diering, G.H., Nirujogi, R.S., Roth, R.H., Worley, P.F., Pandey, A., and Huganir, R.L. (2017). Homer1a drives homeostatic scaling-down of excitatory synapses during sleep. Science *355*, 511-515.

Donnelly, M.L., Luke, G., Mehrotra, A., Li, X., Hughes, L.E., Gani, D., and Ryan, M.D. (2001). Analysis of the aphthovirus 2A/2B polyprotein 'cleavage' mechanism indicates not a proteolytic reaction, but a novel translational effect: a putative ribosomal 'skip'. J Gen Virol *82*, 1013-1025.

Dorrbaum, A.R., Alvarez-Castelao, B., Nassim-Assir, B., Langer, J.D., and Schuman, E.M. (2020). Proteome dynamics during homeostatic scaling in cultured neurons. Elife *9*.

Ehlers, M.D. (2003). Activity level controls postsynaptic composition and signaling via the ubiquitin-proteasome system. Nat Neurosci *6*, 231-242.

Erreger, K., Dravid, S.M., Banke, T.G., Wyllie, D.J., and Traynelis, S.F. (2005). Subunit-specific gating controls rat NR1/NR2A and NR1/NR2B NMDA channel kinetics and synaptic signalling profiles. J Physiol *563*, 345-358.

Fiore, R., Rajman, M., Schwale, C., Bicker, S., Antoniou, A., Bruehl, C., Draguhn, A., and Schratt, G. (2014). MiR-134-dependent regulation of Pumilio-2 is necessary for homeostatic synaptic depression. EMBO J *33*, 2231-2246.

Fujii, H., Inoue, M., Okuno, H., Sano, Y., Takemoto-Kimura, S., Kitamura, K., Kano, M., and Bito, H. (2013). Nonlinear decoding and asymmetric representation of neuronal input information by CaMKIIalpha and calcineurin. Cell Rep *3*, 978-987.

Giese, K.P., and Mizuno, K. (2013). The roles of protein kinases in learning and memory. Learn Mem *20*, 540-552.

Goold, C.P., and Nicoll, R.A. (2010). Single-cell optogenetic excitation drives homeostatic synaptic depression. Neuron *68*, 512-528.

Govindarajan, A., Israely, I., Huang, S.Y., and Tonegawa, S. (2011). The dendritic branch is the preferred integrative unit for protein synthesis-dependent LTP. Neuron *69*, 132-146.

Harvey, C.D., and Svoboda, K. (2007). Locally dynamic synaptic learning rules in pyramidal neuron dendrites. Nature *450*, 1195-1200.

Harvey, C.D., Yasuda, R., Zhong, H., and Svoboda, K. (2008). The spread of Ras activity triggered by activation of a single dendritic spine. Science *321*, 136-140.

Hedrick, N.G., Harward, S.C., Hall, C.E., Murakoshi, H., McNamara, J.O., and Yasuda, R. (2016). Rho GTPase complementation underlies BDNF-dependent homo- and heterosynaptic plasticity. Nature *538*, 104-108.

Herring, B.E., and Nicoll, R.A. (2016). Long-Term Potentiation: From CaMKII to AMPA Receptor Trafficking. Annu Rev Physiol *78*, 351-365.

Hobbiss, A.F., Ramiro-Cortes, Y., and Israely, I. (2018). Homeostatic Plasticity Scales Dendritic Spine Volumes and Changes the Threshold and Specificity of Hebbian Plasticity. iScience *8*, 161-174.

Hochreiter, B., Garcia, A.P., and Schmid, J.A. (2015). Fluorescent proteins as genetically encoded FRET biosensors in life sciences. Sensors (Basel) *15*, 26281-26314.

Hu, J.H., Park, J.M., Park, S., Xiao, B., Dehoff, M.H., Kim, S., Hayashi, T., Schwarz, M.K., Huganir, R.L., Seeburg, P.H.*, et al.* (2010). Homeostatic scaling requires group I mGluR activation mediated by Homer1a. Neuron *68*, 1128-1142.

Jourdain, P., Fukunaga, K., and Muller, D. (2003). Calcium/calmodulin-dependent protein kinase II contributes to activity-dependent filopodia growth and spine formation. J Neurosci *23*, 10645-10649.

Kawashima, T., Kitamura, K., Suzuki, K., Nonaka, M., Kamijo, S., Takemoto-Kimura, S., Kano, M., Okuno, H., Ohki, K., and Bito, H. (2013). Functional labeling of neurons and their projections using the synthetic activity-dependent promoter E-SARE. Nat Methods *10*, 889-895.

Keck, T., Hubener, M., and Bonhoeffer, T. (2017). Interactions between synaptic homeostatic mechanisms: an attempt to reconcile BCM theory, synaptic scaling, and changing excitation/inhibition balance. Curr Opin Neurobiol *43*, 87-93.

Kruijssen, D.L.H., and Wierenga, C.J. (2019). Single Synapse LTP: A Matter of Context? Front Cell Neurosci *13*, 496.

Lee, K.J., Lee, Y., Rozeboom, A., Lee, J.Y., Udagawa, N., Hoe, H.S., and Pak, D.T. (2011). Requirement for Plk2 in orchestrated ras and rap signaling, homeostatic structural plasticity, and memory. Neuron *69*, 957-973.

Lee, M.C., Yasuda, R., and Ehlers, M.D. (2010). Metaplasticity at single glutamatergic synapses. Neuron *66*, 859-870.

Li, X., Zhao, X., Fang, Y., Jiang, X., Duong, T., Fan, C., Huang, C.C., and Kain, S.R. (1998). Generation of destabilized green fluorescent protein as a transcription reporter. J Biol Chem *273*, 34970-34975.

Lisman, J., Yasuda, R., and Raghavachari, S. (2012). Mechanisms of CaMKII action in long-term potentiation. Nat Rev Neurosci *13*, 169-182.

Litwin-Kumar, A., and Doiron, B. (2014). Formation and maintenance of neuronal assemblies through synaptic plasticity. Nat Commun *5*, 5319.

Liu, L., Wong, T.P., Pozza, M.F., Lingenhoehl, K., Wang, Y., Sheng, M., Auberson, Y.P., and Wang, Y.T. (2004). Role of NMDA receptor subtypes in governing the direction of hippocampal synaptic plasticity. Science *304*, 1021-1024.

Lledo, P.M., Hjelmstad, G.O., Mukherji, S., Soderling, T.R., Malenka, R.C., and Nicoll, R.A. (1995). Calcium/calmodulin-dependent kinase II and long-term potentiation enhance synaptic transmission by the same mechanism. Proc Natl Acad Sci U S A *92*, 11175-11179.

Lock, M., Alvira, M., Vandenberghe, L.H., Samanta, A., Toelen, J., Debyser, Z., and Wilson, J.M. (2010). Rapid, simple, and versatile manufacturing of recombinant adeno-associated viral vectors at scale. Hum Gene Ther *21*, 1259-1271.

Malinow, R., and Malenka, R.C. (2002). AMPA receptor trafficking and synaptic plasticity. Annu Rev Neurosci *25*, 103-126.

Marder, E., and Prinz, A.A. (2002). Modeling stability in neuron and network function: the role of activity in homeostasis. Bioessays *24*, 1145-1154.

Matsuzaki, M., Ellis-Davies, G.C., Nemoto, T., Miyashita, Y., Iino, M., and Kasai, H. (2001). Dendritic spine geometry is critical for AMPA receptor expression in hippocampal CA1 pyramidal neurons. Nat Neurosci *4*, 1086-1092.

Matsuzaki, M., Honkura, N., Ellis-Davies, G.C., and Kasai, H. (2004). Structural basis of long-term potentiation in single dendritic spines. Nature *429*, 761-766.

Mendez, P., De Roo, M., Poglia, L., Klauser, P., and Muller, D. (2010). N-cadherin mediates plasticity-induced long-term spine stabilization. J Cell Biol *189*, 589-600.

Mendez, P., Stefanelli, T., Flores, C.E., Muller, D., and Luscher, C. (2018). Homeostatic Plasticity in the Hippocampus Facilitates Memory Extinction. Cell Rep *22*, 1451-1461.

Miller, K.D. (1996). Synaptic economics: competition and cooperation in synaptic plasticity. Neuron *17*, 371-374.

Monyer, H., Burnashev, N., Laurie, D.J., Sakmann, B., and Seeburg, P.H. (1994). Developmental and regional expression in the rat brain and functional properties of four NMDA receptors. Neuron *12*, 529-540.

Morishita, W., Lu, W., Smith, G.B., Nicoll, R.A., Bear, M.F., and Malenka, R.C. (2007). Activation of NR2B-containing NMDA receptors is not required for NMDA receptor-dependent long-term depression. Neuropharmacology *52*, 71-76.

Moulin, T.C., Petiz, L.L., Rayee, D., Winne, J., Maia, R.G., Lima da Cruz, R.V., Amaral, O.B., and Leao, R.N. (2019). Chronic in vivo optogenetic stimulation modulates neuronal excitability, spine morphology, and Hebbian plasticity in the mouse hippocampus. Hippocampus *29*, 755-761.

Murakoshi, H., Shin, M.E., Parra-Bueno, P., Szatmari, E.M., Shibata, A.C., and Yasuda, R. (2017). Kinetics of Endogenous CaMKII Required for Synaptic Plasticity Revealed by Optogenetic Kinase Inhibitor. Neuron *94*, 37-47 e35.

Murakoshi, H., Wang, H., and Yasuda, R. (2011). Local, persistent activation of Rho GTPases during plasticity of single dendritic spines. Nature *472*, 100-104.

Nakahata, Y., and Yasuda, R. (2018). Plasticity of Spine Structure: Local Signaling, Translation and Cytoskeletal Reorganization. Front Synaptic Neurosci *10*, 29.

Nishiyama, J., and Yasuda, R. (2015). Biochemical Computation for Spine Structural Plasticity. Neuron *87*, 63-75.

Noguchi, J., Matsuzaki, M., Ellis-Davies, G.C., and Kasai, H. (2005). Spine-neck geometry determines NMDA receptor-dependent Ca^{2+} signaling in dendrites. Neuron *46*, 609-622.

Oh, W.C., Parajuli, L.K., and Zito, K. (2015). Heterosynaptic structural plasticity on local dendritic segments of hippocampal CA1 neurons. Cell Rep *10*, 162-169.

Okuno, H., Akashi, K., Ishii, Y., Yagishita-Kyo, N., Suzuki, K., Nonaka, M., Kawashima, T., Fujii, H., Takemoto-Kimura, S., Abe, M.*, et al.* (2012). Inverse synaptic tagging of inactive synapses via dynamic interaction of Arc/Arg3.1 with CaMKIIbeta. Cell *149*, 886-898.

Peebles, C.L., Yoo, J., Thwin, M.T., Palop, J.J., Noebels, J.L., and Finkbeiner, S. (2010). Arc regulates spine morphology and maintains network stability in vivo. Proc Natl Acad Sci U S A *107*, 18173-18178.

Perez-Otano, I., and Ehlers, M.D. (2005). Homeostatic plasticity and NMDA receptor trafficking. Trends Neurosci *28*, 229-238.

Pettit, D.L., Perlman, S., and Malinow, R. (1994). Potentiated transmission and prevention of further LTP by increased CaMKII activity in postsynaptic hippocampal slice neurons. Science *266*, 1881-1885.

Philpot, B.D., Cho, K.K., and Bear, M.F. (2007). Obligatory role of NR2A for metaplasticity in visual cortex. Neuron *53*, 495-502.

Philpot, B.D., Sekhar, A.K., Shouval, H.Z., and Bear, M.F. (2001). Visual experience and deprivation bidirectionally modify the composition and function of NMDA receptors in visual cortex. Neuron *29*, 157-169.

Pologruto, T.A., Sabatini, B.L., and Svoboda, K. (2003). ScanImage: flexible software for operating laser scanning microscopes. Biomed Eng Online *2*, 13.

Prybylowski, K., Fu, Z., Losi, G., Hawkins, L.M., Luo, J., Chang, K., Wenthold, R.J., and Vicini, S. (2002). Relationship between availability of NMDA receptor subunits and their expression at the synapse. J Neurosci *22*, 8902-8910.

Quinlan, E.M., Philpot, B.D., Huganir, R.L., and Bear, M.F. (1999). Rapid, experience-dependent expression of synaptic NMDA receptors in visual cortex in vivo. Nat Neurosci *2*, 352-357.

Sabatini, B.L., Oertner, T.G., and Svoboda, K. (2002). The life cycle of Ca^{2+} ions in dendritic spines. Neuron *33*, 439-452.

Sala, C., Futai, K., Yamamoto, K., Worley, P.F., Hayashi, Y., and Sheng, M. (2003). Inhibition of dendritic spine morphogenesis and synaptic transmission by activity-inducible protein Homer1a. J Neurosci *23*, 6327-6337.

Saneyoshi, T., Matsuno, H., Suzuki, A., Murakoshi, H., Hedrick, N.G., Agnello, E., O'Connell, R., Stratton, M.M., Yasuda, R., and Hayashi, Y. (2019). Reciprocal Activation within a Kinase-Effector Complex Underlying Persistence of Structural LTP. Neuron *102*, 1199-1210 e1196.

Schanzenbacher, C.T., Langer, J.D., and Schuman, E.M. (2018). Time- and polarity-dependent proteomic changes associated with homeostatic scaling at central synapses. Elife *7*.

Schanzenbacher, C.T., Sambandan, S., Langer, J.D., and Schuman, E.M. (2016). Nascent Proteome Remodeling following Homeostatic Scaling at Hippocampal Synapses. Neuron *92*, 358-371.

Seeburg, D.P., and Sheng, M. (2008). Activity-Induced Polo-Like Kinase 2 Is Required for Homeostatic Plasticity of Hippocampal Neurons during Epileptiform Activity. The Journal of Neuroscience *28*, 6583-6591.

Shaner, N.C., Campbell, R.E., Steinbach, P.A., Giepmans, B.N., Palmer, A.E., and Tsien, R.Y. (2004). Improved monomeric red, orange and yellow fluorescent proteins derived from Discosoma sp. red fluorescent protein. Nat Biotechnol *22*, 1567-1572.

Sheng, M., Cummings, J., Roldan, L.A., Jan, Y.N., and Jan, L.Y. (1994). Changing subunit composition of heteromeric NMDA receptors during development of rat cortex. Nature *368*, 144-147.

Shepherd, J.D., Rumbaugh, G., Wu, J., Chowdhury, S., Plath, N., Kuhl, D., Huganir, R.L., and Worley, P.F. (2006). Arc/Arg3.1 mediates homeostatic synaptic scaling of AMPA receptors. Neuron *52*, 475-484.

Shibata, A.C.E., Ueda, H.H., Eto, K., Onda, M., Sato, A., Ohba, T., Nabekura, J., and Murakoshi, H. (2021). Photoactivatable CaMKII induces synaptic plasticity in single synapses. Nat Commun *12*, 751.

Shipton, O.A., and Paulsen, O. (2014). GluN2A and GluN2B subunit-containing NMDA receptors in hippocampal plasticity. Philos Trans R Soc Lond B Biol Sci *369*, 20130163.

Sinnen, B.L., Bowen, A.B., Forte, J.S., Hiester, B.G., Crosby, K.C., Gibson, E.S., Dell'Acqua, M.L., and Kennedy, M.J. (2017). Optogenetic Control of Synaptic Composition and Function. Neuron *93*, 646-660 e645.

Snyder, E.M., Philpot, B.D., Huber, K.M., Dong, X., Fallon, J.R., and Bear, M.F. (2001). Internalization of ionotropic glutamate receptors in response to mGluR activation. Nat Neurosci *4*, 1079-1085.

Sobczyk, A., Scheuss, V., and Svoboda, K. (2005). NMDA receptor subunit-dependent [Ca2+] signaling in individual hippocampal dendritic spines. J Neurosci *25*, 6037-6046.

Steiner, P., Higley, M.J., Xu, W., Czervionke, B.L., Malenka, R.C., and Sabatini, B.L. (2008). Destabilization of the postsynaptic density by PSD-95 serine 73 phosphorylation inhibits spine growth and synaptic plasticity. Neuron *60*, 788-802.

Stoppini, L., Buchs, P.A., and Muller, D. (1991). A simple method for organotypic cultures of nervous tissue. J Neurosci Methods *37*, 173-182.

Suarez, L.M., Cid, E., Gal, B., Inostroza, M., Brotons-Mas, J.R., Gomez-Dominguez, D., de la Prida, L.M., and Solis, J.M. (2012). Systemic injection of kainic acid differently affects LTP magnitude depending on its epileptogenic efficiency. PLoS One *7*, e48128.

Tanaka, J., Horiike, Y., Matsuzaki, M., Miyazaki, T., Ellis-Davies, G.C., and Kasai, H. (2008). Protein synthesis and neurotrophin-dependent structural plasticity of single dendritic spines. Science *319*, 1683-1687.

Tang, S., and Yasuda, R. (2017). Imaging ERK and PKA Activation in Single Dendritic Spines during Structural Plasticity. Neuron *93*, 1315-1324 e1313.

Tang, Y.P., Shimizu, E., Dube, G.R., Rampon, C., Kerchner, G.A., Zhuo, M., Liu, G., and Tsien, J.Z. (1999). Genetic enhancement of learning and memory in mice. Nature *401*, 63-69.

Tetzlaff, C., Kolodziejski, C., Timme, M., and Worgotter, F. (2011). Synaptic scaling in combination with many generic plasticity mechanisms stabilizes circuit connectivity. Front Comput Neurosci *5*, 47.

Turrigiano, G.G. (2008). The self-tuning neuron: synaptic scaling of excitatory synapses. Cell *135*, 422-435.

van der Linden, J.A., Joels, M., Karst, H., Juta, A.J., and Wadman, W.J. (1993). Bicuculline increases the intracellular calcium response of CA1 hippocampal neurons to synaptic stimulation. Neurosci Lett *155*, 230-233.

Watt, A.J., van Rossum, M.C., MacLeod, K.M., Nelson, S.B., and Turrigiano, G.G. (2000). Activity coregulates quantal AMPA and NMDA currents at neocortical synapses. Neuron *26*, 659-670.

Wayman, G.A., Lee, Y.S., Tokumitsu, H., Silva, A.J., and Soderling, T.R. (2008). Calmodulin-kinases: modulators of neuronal development and plasticity. Neuron *59*, 914-931.

Yashiro, K., and Philpot, B.D. (2008). Regulation of NMDA receptor subunit expression and its implications for LTD, LTP, and metaplasticity. Neuropharmacology *55*, 1081-1094.

Yasuda, R., Hayashi, Y., and Hell, J.W. (2022). CaMKII: a central molecular organizer of synaptic plasticity, learning and memory. Nat Rev Neurosci *23*, 666-682.

Yoshioka-Kobayashi, K., Matsumiya, M., Niino, Y., Isomura, A., Kori, H., Miyawaki, A., and Kageyama, R. (2020). Coupling delay controls synchronized oscillation in the segmentation clock. Nature *580*, 119-123.

Zenke, F., Agnes, E.J., and Gerstner, W. (2015). Diverse synaptic plasticity mechanisms orchestrated to form and retrieve memories in spiking neural networks. Nat Commun *6*, 6922.

Zenke, F., Hennequin, G., and Gerstner, W. (2013). Synaptic plasticity in neural networks needs homeostasis with a fast rate detector. PLoS Comput Biol *9*, e1003330.